Brittle Shear Tectonics in a Narrow Continental Rift: Asymmetric Nonvolcanic Barmer Basin (Rajasthan, India)

Swagato Dasgupta[1] *and Soumyajit Mukherjee*[2,*]

1. Reliance Industries Limited, Ghansoli, Navi Mumbai 400 701, Maharashtra, India; 2. Department of Earth Sciences, Indian Institute of Technology Bombay, Powai, Mumbai 400 076, Maharashtra, India

ABSTRACT

Our field studies emphasizing brittle shear P- and Y-planes along the margins of the Barmer basin (Rajasthan, India) support its two-phase (NW-SE, followed by NE-SW) extension during Early Cretaceous and Late Cretaceous–Paleocene periods. We also document nearly NE-trending megascale transfer zones along the northern margin of the Barmer basin. Preexisting brittle planes in the Malani basement rocks guided the relay structures here. Structures at the western basin shoulder margin indicate NE-SW extension, and the crosscut relation connotes the relative timing of the two extension phases. The crosscutting conjugate fault sets are non-Andersonian. The NW-trending faults produced by the second-phase extension and the inherited NNW-trending brittle features are dominantly dip-slip. Prior fractures of the Malani rocks at ≥45° to the NE-SW principal extension direction extended the Barmer basin obliquely during the Late Cretaceous–Paleocene period. The asymmetric nature of the rift, too, connotes its oblique rifting. The extension direction of the first phase probably rotated clockwise. This is derived mainly from WSW-trending faults cutting NE-trending faults. Brittle planes of shear and fracture significantly promoted fluid flow, as understood from secondary hydrothermal mineral deposits (Barmer hill area) and pre-Deccan basalts (Sarnoo area). Reverse slip detected along subvertical faults on the western and eastern rift shoulders are probably due to isostatic flexure–related contraction or might be related to the far-field effect of ridge-push forces. The Mesozoic subsurface stratigraphy there and elsewhere within the Barmer basin requires more study to substantiate the potential for structural entrapment of hydrocarbon.

Online enhancements: appendix.

Introduction

Rifting of continental crust is one of the key geodynamic processes that evolve continental lithosphere and generate oceanic basins. Extension and crustal thinning can develop by upwelling of a mantle plume (active rifting; Luhr et al. 1985; Wright et al. 2016) or by regional stresses originating presumably from distant plate boundary–related forces (passive rifting; Ruppel 1995; Corti et al. 2003; Koptev et al. 2015). In active rifts associated with a rising mantle plume, the crust arches over the upwelling mantle. This is followed by voluminous surficial volcanism. In passive rifting, tensional regional stress dominantly thins the crust, producing a rift basin. In the second case, crustal thinning may cause passive rising of mantle that underplates lithospheric magma and may lead to eruption of flood basalts, inducing a strong thermal gradient (Corti et al. 2003).

Effects of lithospheric flexure and its relations with other dynamic processes (Buck 1988) are observed in both volcanic and sedimentary rift basins, both along continental plate margins and in the interior (Watts 2001; Ziegler and Cloetingh 2004). A continental rift flank may be uplifted by mechanical unloading of the footwall block by normal faulting associated with erosion and sedimentation (Weissel and Karner 1989; as reviewed in Watts 2001). Crustal heat flow plays a major role in rift tectonics. In low- to moderate-heat-flow areas within continental crust, brittle upper and ductile lower crusts couple strongly. In such cases, the lower crust will thin homogeneously (Whitney et al. 2013) and a number of normal faults will generate

Manuscript received December 28, 2016; accepted May 26, 2017; electronically published August 3, 2017.

* Author for correspondence; e-mail: soumyajitm@gmail.com.

[The Journal of Geology, 2017, volume 125, p. 561–591] 0022-1376/2017/12505-0006$15.00. DOI: 10.1086/693095

half- to full grabens in the brittle upper crust, with younger faults crosscutting older ones (Brady et al. 2000). On the other hand, comparatively hot brittle upper crust decouples mechanically from the ductile lower crust (Ricketts et al. 2015), and strain localizes along a single steep normal fault with large throw that temporally gets gentler with isostatic rebound (Wdowinski and Axen 1992; Ricketts et al. 2015). Such high-angle normal faults get younger toward the basin axis (Ricketts et al. 2015). With an increase in isostatic rebound, the ductile lower crust may be exhumed to the surface as a core complex (Ricketts et al. 2015).

The modes of continental rift segmentation and discontinuous propagation are guided by preexisting basement structures, and this process is called "tectonic inheritance" (Fossen 2013; recent reviews in Misra and Mukherjee 2015 and Robertson et al. 2016). Inherited structures develop from preexisting fabrics such as foliation, lineation, and fractures (Swanson 1986). Weaker zones having preexisting fabrics, such as the underlying Archean-Proterozoic mobile belts, govern how rift faults propagate. The geometry of the fault planes originating from preexisting structures in anisotropic rocks does not necessarily follow Coulomb's failure criterion and Andersonian faulting. These are termed non-Andersonian faults (Brune and Autin 2013). The basement anisotropies and/or discontinuity surfaces affect the rock strength and rheology (Morley et al. 2004; Misra and Mukherjee 2015). Rift faults splay out in the vicinity of the preexisting structures/shear zones. Thus, accommodation zones/transfer zones (Gawthorpe and Hurst 1993; Morley 1995, 1999) are created where the rift-related faults intersect the preexisting zone of weakness. Such transfer zones, in many cases, are hard-linked and associated with a strike-slip component along the preexisting structures. Experiments show that coupled systems are more likely to connect the younger rift-related faults to preexisting, reactivated basement-related faults, whereas in the decoupled systems the younger faults develop and reactivate preexisting basement faults but do not necessarily connect them (Richard and Krantz 1991).

Continental extension can be in the form of narrow or wide rifts. Narrow rifts can be a maximum of 100–150 km wide, categorized by thinning of crustal and lithospheric mantle and intense steeply dipping normal faults (Buck 1991; Corti et al. 2003). Such narrow rift zones generally have distinct lateral variation of crustal thickness associated with heat flow higher than that in the rift shoulders. Transfer zones significantly accommodate differential displacement along the rift axes. On the other hand, wide rifts consist of several disconnected basins extending across more than 1000 km (Corti et al. 2003). The lateral variation of crustal thickness is relatively small, produced by a uniform crustal and lithospheric mantle thinning (Corti et al. 2003). Wide rifts are thus associated with strong continental crust (Buck 1991).

Many continental rift margins undergo strike-slip controlled deformation associated with transtention and/or transpression basins (e.g., Nemčok 2016). Such strike-slip regimes uplift basement ridges as well as create new accommodation space by transfer faults. Thus, in many cases, strike-slip systems develop compressional features associated with reverse faulting: basins in the equatorial Atlantic region, the Fundy rift basin of SE Canada, and the East Africa rift system (Gibbs 1984; McClay 1990; Ring et al. 1992; Withjack et al. 1995, 1998, 2002; McClay and Bonora 2001; Lezzar et al. 2002; Nemčok et al. 2012; Nemčok 2016). Besides the strike-slip component, reverse faults in extensional basin margins can also form by basin inversion due to extension followed by compression (Schlische 1995), as in eastern North America, the Missour basin in Morocco, the Rio Grande rift of central New Mexico, the Kutch rift basin of western India, the Sierras Pampeanas of Córdoba in Argentina, and the Faeroe-Shetland Basin in the northern offshore part of United Kingdom (Chamberlin 1983; Chung and Gao 1995; Beauchamp et al. 1996; Withjack et al. 1998; Davies et al. 2004; Biswas 2005; Ricketts et al. 2015; Martino et al. 2016). It is not necessary that only compressive forces related to strike-slip and collision/subduction would result in reverse faulting and/or inversion in an extensional setting. Extensional stress associated with far-field ridge-push forces along seafloor spreading margins also produces reverse faulting along the continental rift margins, for example, the Fundy rift basin (Canada; Withjack et al. 1995). Other than this, isostatic flexture–related contraction in uplifted footwall can also result in reverse faulting (e.g., the Rio Grande rift margin; Lewis and Baldridge 1994).

Three sedimentary basins—Jaisalmer, Barmer, and Bikaner-Nagaur—outcrop in western Rajasthan, India (fig. 1; Dasgupta 1975; Pandey and Bhadu 2010; Arora et al. 2011; Singh and Tewari 2011). The former two basins consist of thick Mesozoic and Tertiary sediments (Biswas 2012; Dwivedi 2016). The Barmer failed narrow-rift basin is ~200 km long along the NNW and is ~50 km wide (fig 1*A*); it is separated from the Jaisalmer basin on the north by the NE-trending Devikot-Fatehgarh/Barmer-Devikot-Nachana ridge/structural high (Misra et al. 1993; Compton 2009; Bladon et al. 2015; Dolson et al. 2015). Distinct Bouguer anomaly gravity lows along the Cambay basin extend into the Barmer rift basin, accompanied by high-amplitude gravity highs along the rift

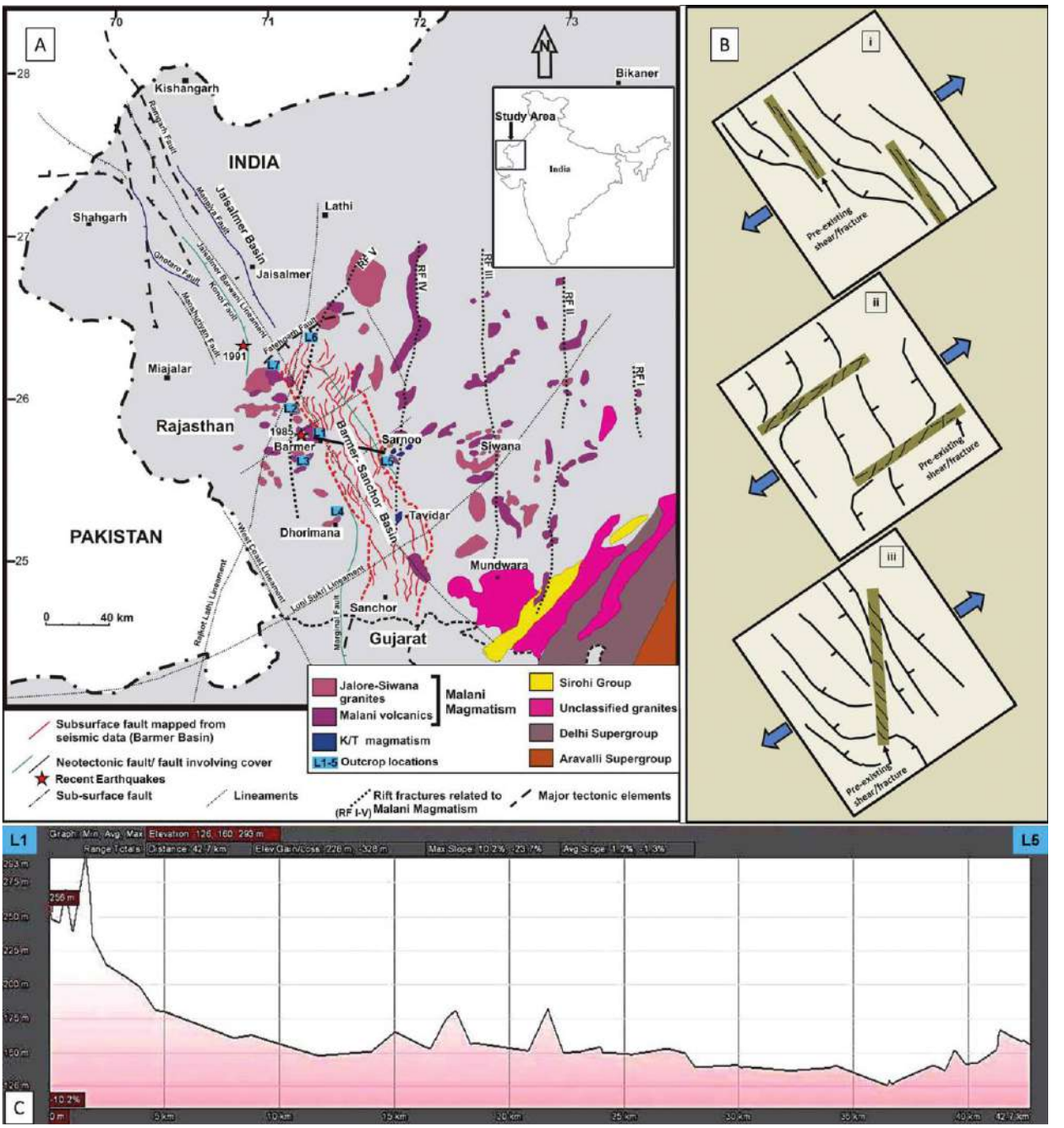

Figure 1. *A*, Geological map of western Rajasthan, depicting the Barmer/Barmer-Sanchor basin (see inset for location in India) along with different fault trends: subsurface faults mapped in seismic data, neotectonic and other lineaments, and the rift fracture trend of the Malani Igneous Suite (MIS) and other major tectonic elements (compiled and modified from Misra et al. 1993; Bhushan 2000; Dasgupta et al. 2000; Sharma 2005; Roy 2006; Kilaru et al. 2013; Sinha-Roy et al. 2013; Bladon et al. 2014, 2015). Field outcrop locations are marked on the map along the periphery of the Barmer basin. Locations L1–L4 are at the western margin, L5 at the eastern margin, and L6 and L7 at the northern margin. RF = rift fractures of the MIS. Recent earthquakes occurred in 1985 and 1991 (Joshi et al. 1997) in surrounding areas (coordinates obtained from www.earthquaketract.com). *B*, Schematic sketch depicting the interaction of rift-related faults and pre-existing shear/fracture with respect to the extension direction (blue arrows). The angle (θ) between preexisting shear/fracture and extension direction is 90° (*i*), 0° (*ii*), and $0° < \theta < 90°$ (*iii*; modified from Morley et al. 2004; also see Misra and Mukherjee 2015). *C*, An elevation profile from NW to SE (L1–L5) across the Barmer basin rift shoulders, extracted from Google Earth Pro, depicts the rift basin to be asymmetric.

shoulders on either side. The gravity low at the Jaisalmer basin is separated by a prominent gravity high in the Barmer basin. The residual magnetic anomaly maps also depict this (Mishra 2011). The NE-trending gravity and magnetic anomalies in the Barmer region indicate low-amplitude basement highs and lows. The magnetic anomalies associated with the Barmer rift basin shoulders have high amplitudes that diminish in the residual anomaly map. This indicates that the rift basin is coeval with mafic intrusion (Mishra 2011). The Mesozoic Barmer rift basin was reactivated during the early Tertiary by Deccan volcanism (Mishra 2011). A modeled NE-SW cross section from the Bouguer anomaly map across the Barmer basin identifies a mafic basement with voluminous intrusion and Moho upwelling up to 27–28 km beneath the basin—typically a rift basin setup (Mishra 2011).

A subsurface fault map from seismic data indicates transfer zones mainly in the northern and eastern parts of the Barmer basin (Bladon et al. 2014, 2015). Transfer zone and relay structures play key roles in rift faulting and sedimentation. The Mesozoic succession of the Barmer basin outcrops at the eastern rift shoulder near Sarnoo village. This Early Cretaceous sedimentary unit was deposited as a result of transtensional extension during the Madagascar separation (Bladon et al. 2014). This resulted in NE- and nearly east-trending faults, which were later superimposed by NW-trending faults during the main Barmer rift episode in the Late Cretaceous to Paleocene. Thus, it is observed that the Barmer basin involves preexisting rift fractures/faults trending to the NE related to Mesozoic extension and also older Malani-equivalent rift fractures trending nearly north to NNE. Figure 1*B* presents the interaction of rift-related faults and preexisting shears/fractures with respect to the main Barmer rift extension direction.

Motivation for Studying Barmer Basin

Rift kinematic analysis is of great interest in petroleum geosciences (e.g., Misra et al. 2014; Misra and Mukherjee 2015). It explains the timing and pattern of faults and the possible nature and timing of fault reactivation (Bellahsen and Daniel 2005). These are also the governing elements for pore fluid flow (Caine and Forster 1999) and reservoir development. We study structures along the rift margin of the Barmer basin from the field and address (1) whether the rift shoulder (fig. 1*A*, 1*C*) trends match with the main Barmer rift, (2) whether extension affected the rift shoulder, (3) the nature and relative timing of rifting in relation to Deccan volcanism, and (4) whether the brittle planes (fractures and faults) around the rift shoulder and margin indicate the effect of tectonic inheritance from the Malani rocks. Three possibilities exist regarding fault-plane orientation to stress direction in rift tectonics (fig. 1*B*); we discuss which possibility is more likely. In addition, we address (5) the presence of any reverse faulting and its probable cause.

Tectonics and stratigraphy of the NW segment of India range from the Precambrian to the Cenozoic. Some of the distinct Phanerozoic rift basins of western Rajasthan (Biswas 1999) developed over the Malani igneous province/rhyolites linked with the separation of the Indian plate from Gondwanaland during the Mesozoic (review in Valdiya 2010, p. 363–365). The Barmer rift, also known as the Barmer-Sanchor rift, extends southward up to the locality Sanchor (fig. 1*A*), beyond which it merges with the NNW/north-trending Cambay rift system. The basin deepens toward the south/SE. This basin was much less explored earlier; however, during the past decade it turned out to be one of the major prospective petroleum basins (Farrimond et al. 2015; Kothari et al. 2015), with reserves of more than 1 billion barrels. Therefore, from both academic tectonic and petroleum geological viewpoints, we picked the Barmer basin to study.

Geology

Stratigraphy. The Barmer basin consists of a thick Jurassic to Eocene accumulation of shallow marine to fluvial sedimentary sequences (table A1, available online). The Late Proterozoic Malani igneous suite/rhyolites (MIS) constitute its basement, which is exposed around the western rift shoulder of the Barmer basin. The Fatehgarh and Barmer Hill Formations are the major hydrocarbon reservoirs of the Barmer basin. The Mangala and Aishwarya/Aishwariya oil fields have been producing hydrocarbons from the Barmer Hill Formation (Shiju et al. 2008; Lobo et al. 2015). Figure 2 presents a Wheeler diagram of a chronostratigraphic section, taking into account the available stratigraphic information from current literature (Sisodia and Singh 2000; Mathur 2003; Mathur et al. 2005; Sisodia et al. 2005; Compton 2009; Beaumont et al. 2015; Dolson et al. 2015; Kothari et al. 2015).

Tectonics. The sedimentary basins of Rajasthan (India), west of the Aravalli axial trend, used to be the shelf part of the paleo-Tethys during the Gondwana period. The Jaisalmer basin, with a NW structural trend, had been a part of this broad, stable shelf, which extends and deepens toward the NW into the Indus shelf in Pakistan. Toward the south, the Barmer basin

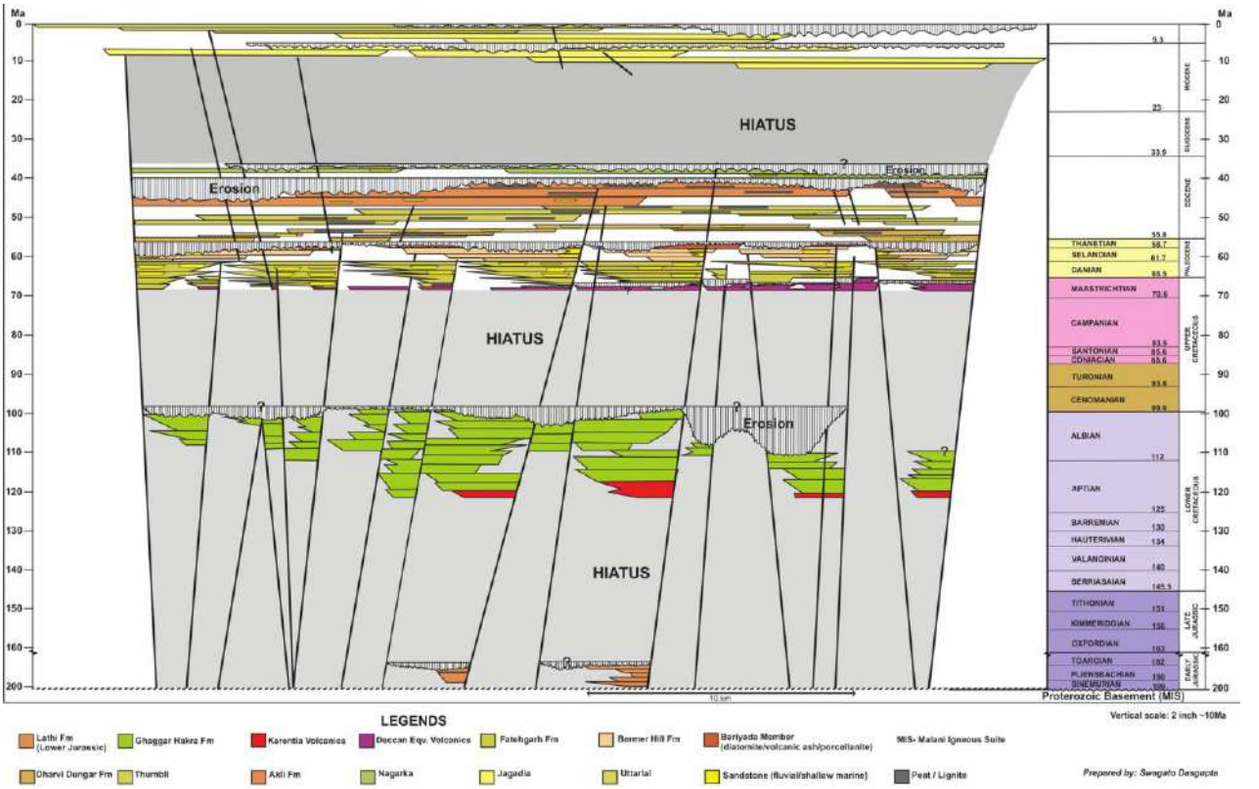

Figure 2. Chronostratigraphic NW-SE section across the Barmer basin (compiled from Sisodia and Singh 2000; Mathur 2003; Mathur et al. 2005; Sisodia et al. 2005; Compton 2009; Dolson et al. 2015; Kothari et al. 2015; John et al. 2017). Major depositional units with respect to geological time associated with prominent erosional events and hiatuses are presented. Deccan Eqv. = Deccan equivalent.

rifted in two distinct phases: (1) NW-SE extension by the east-west Gondwana separation in the Mesozoic and (2) NE-SW extension from the K-T boundary until the Paleocene, as the Seychelles microcontinent separated from India (Sharma 2007; Collier et al. 2008; Mishra 2011; Torsvik et al. 2013; Bladon et al. 2014, 2015). Bladon et al. (2014, 2015) described the rift fault geometry from field and subsurface seismic mapping. The dominant fault system in the Sarnu/Sarnoo hill area at the eastern rift shoulder strikes NE and nearly east, along with cross-trend NW fractures (Bladon et al. 2014). The lower Cretaceous sedimentary sequence of the Sarnoo hill area was probably deposited during transtension linked to the Madagascar separation from the Indian plate (Bladon et al. 2014). On the other hand, the dominant rift-related faults strike NW at the western rift shoulder, the Barmer hill area. Older, nearly north-south-trending Proterozoic rift fractures have also been reported from the Malani basement (Sharma 2005). The eastern margin of the basin is bounded by steep-dipping normal faults that accommodated a thick pile of sediment. Inheritance of preexisting structures associated with relay ramps and transfer zones identified from seismic fault mapping has been documented from the eastern part of the basin (Bladon et al. 2014), whereas the western margin, though fault bound, is affected by flexural uplift due to isostasy. The northern margin is defined by the Devikot-Fatehgarh Fault, which slipped, possibly during the late Tertiary, as a result of Himalayan collisional tectonics (Compton 2009; Mukherjee and Koyi 2010*a*, 2010*b*; van Hinsbergen et al. 2012; Mukherjee 2013*a*, 2015*a*; Mukherjee et al. 2013, 2015; Kelly et al. 2014). The Fatehgarh Formation—the main reservoir system of the Barmer basin—was exposed along this ENE fault trend. Deccan-related volcanism at a few locations close to Sarnoo and Tavidar/Tavider (Bhushan 2000; Sharma 2007; Sheth 2007; Vijayan et al. 2015) relates to reactivation of older crustal fractures within the MIS.

Please note that the appendix, available online, presents structural and tectonic studies by Cairn Energy employees. The sites are from undisclosed GPS locations within the Barmer basin.

Regional Aspects. *The Malani Basement Rock.* The MIS is a heterogeneous group of three-phased ig-

neous rocks consisting of acid plutonic to volcanic flows along with basic groups and is associated with nearly north-south linear trends of basal conglomerate as well as volcanic flows. This indicates that the Malani volcanism was controlled by lineaments related to intracratonic rift zones (Sharma 2005). As previously suggested, this igneous suite is unmetamorphosed and undeformed (Sharma 2005; review in Sisodia 2011). The MIS initiated by extensional tectonics (Axen and Bartley 1997) indicated by north-south subparallel crustal fractures (fig. 1*A*) suggests an intracratonic rifted setting. A few rift fractures in the eastern to SE part of the Barmer basin reactivated during the early Tertiary and/or at the K-T boundary (Torsvik et al. 2001; Sharma 2005), namely, the Sarnu-Dandali and Tavider magmatism (Sen et al. 2012; fig. 1*A*).

The basement gneiss and granitoids of the MIS are intruded by felsic rocks (Pandit et al. 1999). The dikes within the Sankra pluton (Rao et al. 2003) near the Jaisalmer area have a noticeable NNW trend, along with a less prominent NE one. The pole position and magnetic orientation of the Malani rhyolite connote that it is related to Rodinia fragmentation by anorogenic rifting on the NW greater Indian craton (Torsvik et al. 2001; Sharma 2005).

Sarnoo Hill Area. The Barmer rift basin evolved during the Late Cretaceous to Paleocene by NE extension related to separation of the Seychelles microcontinent from the NW Indian plate margin. However, the presence of Early Cretaceous fluvial sandstones in the Sarnoo hill area, at the central eastern rift margin, indicates an older rift phase in the Barmer basin (Bladon et al. 2014; Dolson et al. 2015). The Early Cretaceous sedimentary succession exposed in the Sarnoo hill area belongs to the Ghaggar-Hakra Formation (Baksi and Naskar 1981; Sisodia and Singh 2000). It lies unconformably over a weakly alkaline Aptian intrusive igneous rock (Sharma 2007; Sisodia and Singh 2000). Some igneous intrusions within the sedimentary succession are observed in the Sarnoo hill area, presumably fed by pre-Deccan volcanism (Basu et al. 1993; Roy and Jakhar 2002; Roy 2003). No synkinematic growth sedimentary sequence is observed in the Sarnoo hill area (Bladon et al. 2014).

Devikot-Fatehgarh Ridge. Sedimentary layers of the Barmer basin thin toward the north and are uplifted locally (Compton 2009) along the NE-trending Devikot-Fatehgarh Fault ~100 km north of Barmer. The probable cause of this uplift is the Himalayan orogeny related to the ongoing compression during the late Tertiary (Compton 2009; Kelly et al. 2014). Subsequent erosion of the Late Cretaceous to early Tertiary section developed a fault scarp (Compton 2009) along this NE/ENE trend. The Fatehgarh Sandstone occurs as the lowermost unit of the uplifted section.

Analysis from Remote-Sensing and Field-Based Study

Remote-Sensing Studies. Google Earth Pro images of the year 2016 were used to identify the exposures in and around the Barmer basin. Most of the rocks crop out at the periphery of the rift basin. Seven exposures were studied (fig. 1*A*) at the basin margin: L1 and L2, a set of exposures surrounding the Barmer town and Gehnoo village area toward the west; L3, in and around the Jasai village area farther west; L4, near Dhorimana village, at the western margin toward the south; L5, near Sarnoo village in the eastern rift margin; and L6 and L7, the Devikot-Fatehgarh ridge, toward the north.

Several lineaments were identified in these locations. The major trends are (1) NE, ENE to nearly east, and a few NW in Sarnoo hill area (fig. 3*a*); (2) mainly NW and WNW, along with some NE lineaments, in the MIS outcrop surrounding the Barmer, Jasai, and Dhorimana areas (fig. 3*b*, 3*c*); and (3) a NE-trending, near-linear fault zone extending ~20–23 km along the Devikot-Fatehgarh ridge toward the north (fig. 3*d*). No lineaments could be identified confidently on the possible mafic igneous exposures near the Sarnoo village.

Brittle Shear Features. See figure A1 (figs. A1–A13 available online) for brittle shear feature nomenclature.

Western Margin. The basement rock of Barmer basin, equivalent to the MIS, is exposed in three places.

1. Barmer hill area near Ratanada Temple (fig. 1A). The sedimentary unit, consisting of basal conglomerate overlain by sandstones, truncates onto the lower part of these rhyolite hills (fig. 4). The majority of the primary brittle shear Y-planes (previously called "D-planes"; reviewed in Ghosh 1993; also see Mukherjee 2011, 2012, 2013*b*, 2015*b*; Babar et al. 2017; Kaplay et al. 2017) are subvertical and trend NW (figs. 5, A2; pole plots in fig. 4), subparallel to the Barmer basin trend. Sigmoid brittle P-planes merge with these Y-planes, indicating a consistent sinistral shear. Thus, even though slickensides are not prominent on the Y-planes, it was possible to identify Y- and P-planes simultaneously and decipher slip sense (as in Mukherjee and Koyi 2010*a*, 2010*b*; Mukherjee 2013*c*; Misra et al. 2014; Misra and Mukherjee 2017). White secondary mineralizations of carbonates and kaolinites up to ~1.3–2 cm thick occur within both Y- and P-planes (fig. 5). The mineralizations, themselves devoid of Y- and P-planes, seem to have

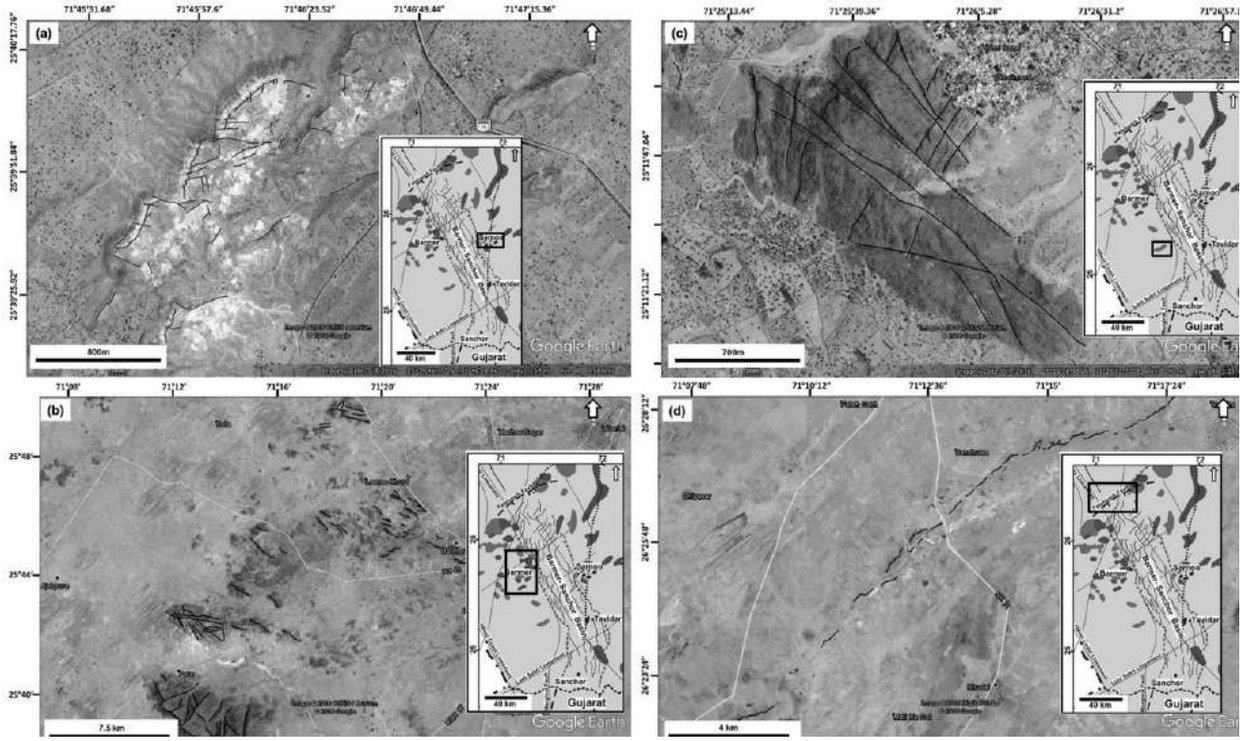

Figure 3. Satellite imagery from Google Earth Pro, showing major lineaments along the western and eastern rift margins. *a*, Sarnu/Sarnoo outcrop area. *b*, Barmer town, Jasai and Gehnoo villages. *c*, Dhorimana area. *d*, Uplifted ridges along the Fatehgarh Fault. A color version of this figure is available online.

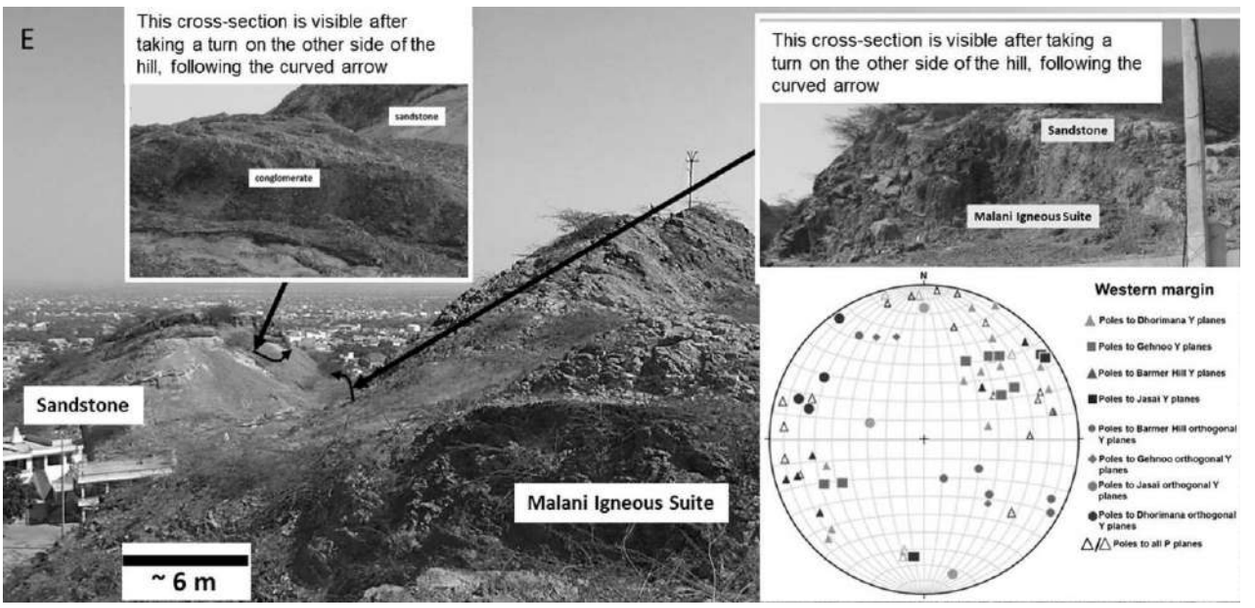

Figure 4. Landscape view of the basement rock—the Malani Igneous Suite (MIS)—exposed west of Barmer town, with synrift succession of basal conglomerates and sandstones truncating against the MIS in the lower part toward the east. Inset: Stereoplot of poles of Y- (filled points) and P- (open points) planes of NW- and NE-trending brittle shear faults, as identified along the western rift shoulder (from the Barmer hill area, Gehnoo village, near Jasai and Dhorimana villages) of the Barmer basin. NE-trending faults are less numerous than those trending NW. A color version of this figure is available online.

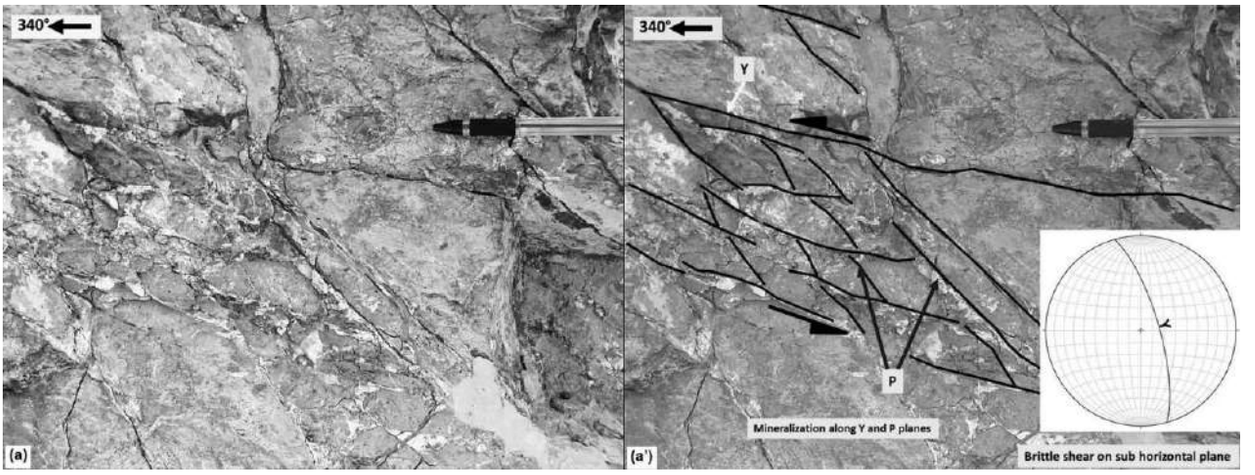

Figure 5. Uninterpreted (*a*) and interpreted (*a*′) outcrop examples of sinistral brittle shear with distinct Y- and P-planes within Malani rhyolites, observed on a subhorizontal surface. The Y-plane trends NW (attitude: 164° strike, 74° dip, 74° dip direction). Mineralization along Y- and P-planes consists mainly of calcite, secondary quartz, and kaolinite. Part of a pen (~12 cm) is shown for scale. Inset: stereoplot of the Y-plane. Location: SW of Ratanada Temple in the Barmer hill area, Barmer town; near L1 in figure 1*A*. A color version of this figure is available online.

been deposited after brittle shear. Neither gouge nor breccia developed along the Y- and P-planes. Faulting within the overlying sandstone layer is much less abundant and is smaller in scale; only fractures are observed at places.

Nearly orthogonal to this, a second set of mostly sinistral brittle strike-slip shear with another set of Y-planes trends NE, and these were also identified in the field on the basis of association with sigmoidal curved P-planes that merge tangentially with the Y-planes (figs. 4, 6). These Y-planes dip 23°–82°. Secondary quartz mineralization as slickensides (Means 1987) on a few Y-planes defines the slip sense. Asymmetric/knobby elevations (type AE-3 in fig. 1 of Doblas 1998) developed on the Y-planes (Doblas 1998) reveal sinistral shear. Slopes of steep surfaces of such elevations indicate the movement direction of the missing block (fig. 7). A less prominent slickenside is observed on a fault plane that trends 243° and dips 23° toward the NW (fig. A3). Southwest-trending (~220°) striations are observed from a part of this fault plane. The striations indicate nearly strike-

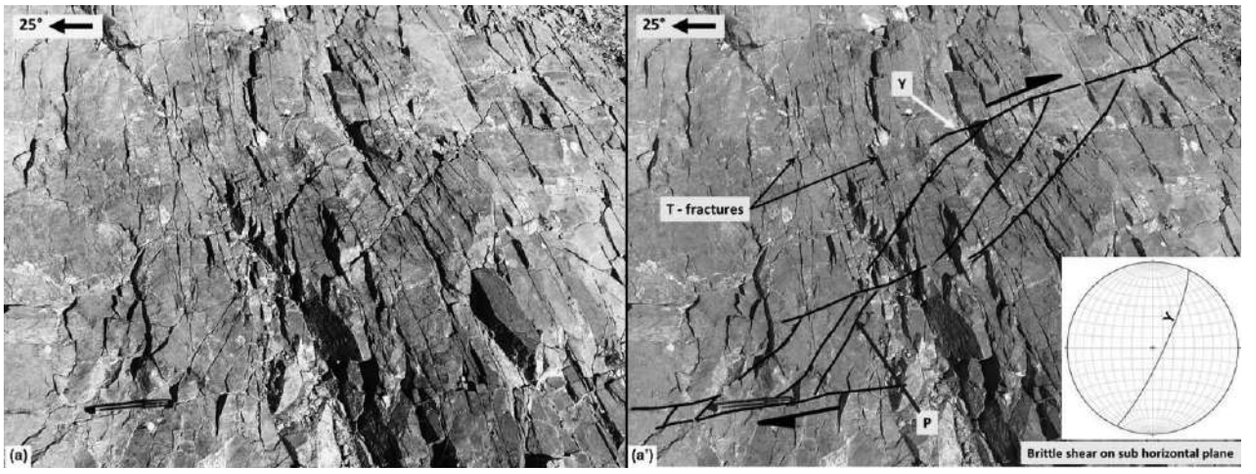

Figure 6. Uninterpreted (*a*) and interpreted (*a*′) outcrop examples of dextral brittle shear with distinct Y- and P-planes within Malani rhyolite observed on subhorizontal surface. The Y-plane trends NE (attitude: 205° strike, 80° dip, 115° dip direction). Subparallel extensional fractures (T-fractures) nearly orthogonal to the Y-planes are seen. A pen ~15 cm long is shown for scale. Inset: stereoplot of the Y-plane. Location: NW of Ratanada Temple in the Barmer hill area, Barmer town; near L1 in figure 1*A*. A color version of this figure is available online.

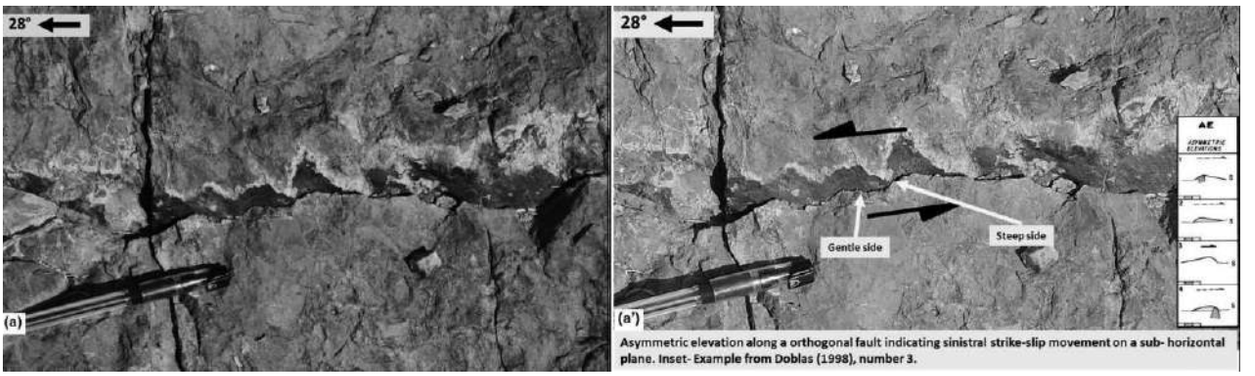

Figure 7. Uninterpreted (*a*) and interpreted (*a*′) outcrop examples of prominent slickensides. Asymmetric elevation connotes sinistral strike-slip movement on subhorizontal surface (Y-plane attitude: 210° strike, 84° dip, 300° dip direction). Inset: asymmetric elevation (AE; no. 3) taken from figure 1 of Doblas (1998). Part of a pen (~13 cm) is shown for scale. Location: west of Ratanada Temple in the Barmer hill area, Barmer town; near L1 in figure 1*A*. A color version of this figure is available online.

slip movement; however, the sense of shear, whether dextral or sinistral, is indeterminate.

Other than slickenside features, extensional fractures are also seen on subhorizontal outcrops associated with a second set of a few NE-trending faults (fig. 6). These fractures are nearly orthogonal to the shear Y-plane having subparallel strike and are nearly equidistant. They are also referred to as "tensional fractures" (T-fractures; not "transgranular fractures"), as they indicate tension perpendicular to their strike. In this area, faults are observed in two ways: (1) as Y- and P-planes exposed as lines in plan views (figs. 5, 6, A2) and (2) as exposed fault planes with local but prominent striations (figs. 7, A3).

Around Gehnoo village (fig. 1*A*), ~30 km NW of Barmer town, a number of brecciated fault gouge zones (fig. 8) exist, resembling those described by Taylor (2009) from different terrains. The brittle shear faults usually trend NW (figs. 4,8, A4), observed on a subvertical plane. Some of these NW-trending faults crosscut the NE-trending top-to-SW (up) orthogonal brittle shears (fig. 8). At places, the NW-trending fault and/or fracture planes were seen in a subvertical plane at two locations, which di-

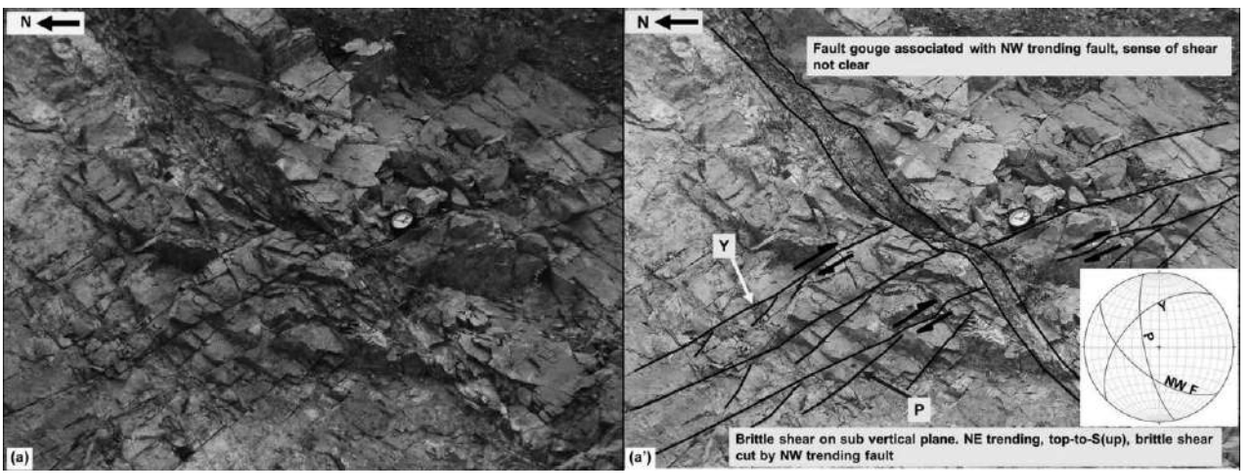

Figure 8. Uninterpreted (*a*) and interpreted (*a*′) photographs of brittle shear features observed on a subvertical surface. A NW-trending fault (attitude: 128° strike, 58° dip, 218° dip direction) with a 10–12-cm-thick fault gouge cuts NE-trending brittle shears with well-developed P-plane (attitude: 168° strike, 74° dip, 258° dip direction) and Y-plane (attitude: 225° strike, 49° dip, 315° dip direction) having top-to-south (up) sense of movement. A pen ~15 cm long and a clinometer ~8 cm in diameter are shown for scale. Inset: stereoplot of the NW-trending fault and the Y- and P-planes of the NE-trending fault. Location: roadside exposure toward Genhoo village; near L2 in figure 1*A*. A color version of this figure is available online.

verge toward the top: a possible appearance of flower structure (fig. A5; e.g., Dewey et al. 1998; Chetty and Rao 2006). These are cross-section views of a strike-slip brittle shear fault associated with Y- and P-planes (Naylor et al. 1986).

2. Jasai hill area (fig. 1A). The outcrop is located ~15 km west of the Barmer rift margin. Malani igneous suite rhyolites occur, along with some melanocratic intrusions. Brittle shear planes/fault planes with usually NW trend are seen on horizontal surfaces with dextral shear (fig. 9). Also, there are some orthogonal faults trending SW (fig. 9), with sinistral shear observed on subhorizontal planes. Such orthogonal faults are also observed on the subvertical surface. These faults trend nearly east or ESE (fig. A6*a*, A6*a*′), with top-to-south (up) shear. Its conjugate set trends nearly north-south, with top-to-NW (up) shear, as seen on a subvertical plane (fig. A6*b*, A6*b*′). Two examples of ~115°-trending dikes of melanocratic rock (dolerite?) with xenoliths of sedimentary rocks intrude along the nearly east-trending Y-plane. These might be Late Proterozoic dikes intruded within the MIS (figures available from authors).

3. Near Dhorimana (fig. 1A). This area is ~10–15 km west of the Barmer rift margin. The major fault subparallels the Barmer rift margin. Pink MIS granite consists of coarse grains of dominantly k-feldspar, quartz, and biotite. Two prominent sets of brittle fault planes are documented. The NW-trending Y-planes are more numerous (figs. 10, 11, A7). Two intersecting near-orthogonal fault planes are observed on a subhorizontal outcrop (fig. 10). The

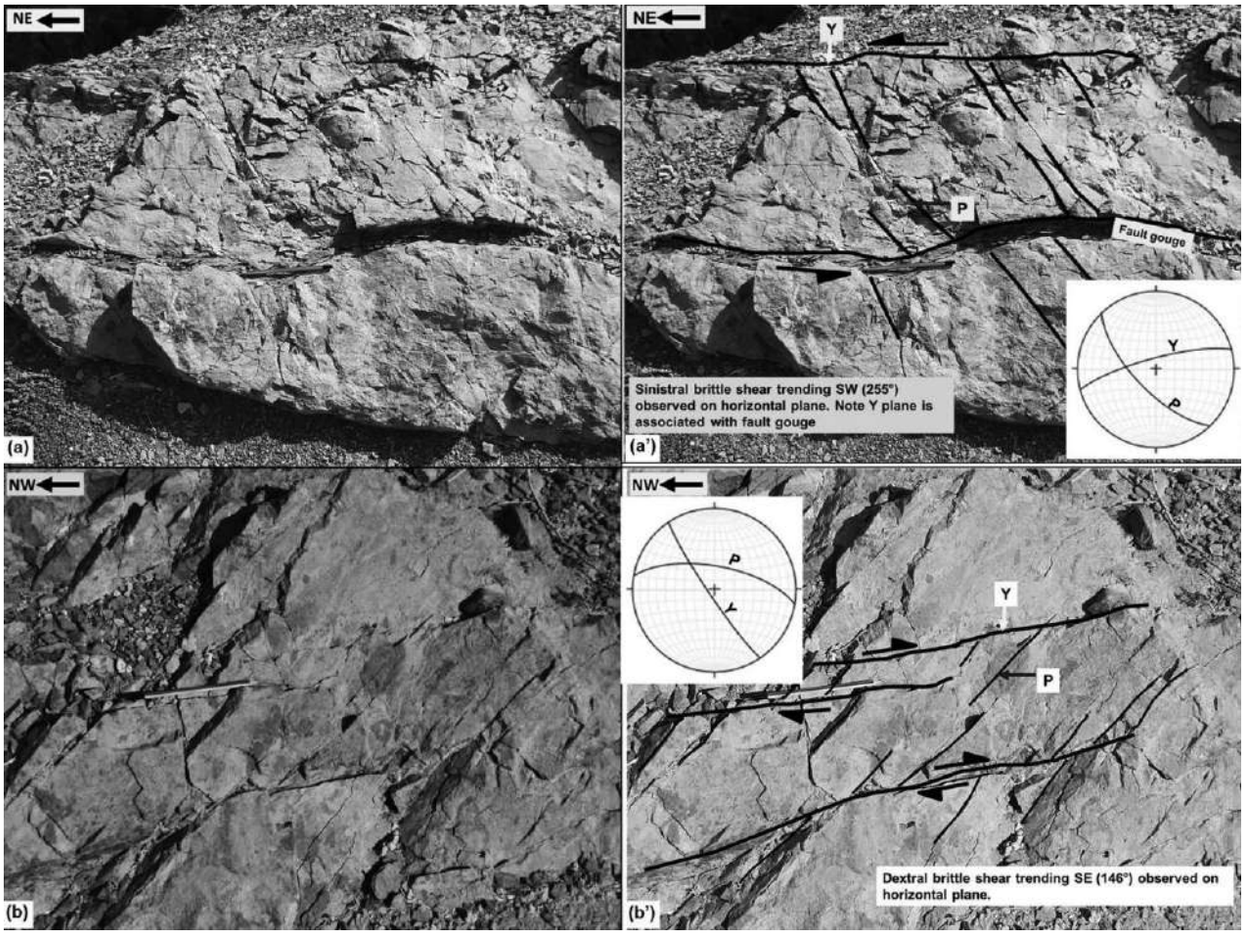

Figure 9. *Top*, uninterpreted (*a*) and interpreted (*a*′) photographs of NE-trending sinistral brittle shear with a P-plane (attitude: 136° strike, 68° dip, 226° dip direction) and a Y-plane (attitude: 255° strike, 78° dip, 345° dip direction) observed on a subhorizontal surface. A 3–5-cm-thick fault gouge is seen along the Y-plane. *Bottom*, uninterpreted (*b*) and interpreted (*b*′) images of NW-trending dextral brittle shear with a P-plane (attitude: 100° strike, 66° dip, 10° dip direction) and a Y-plane (attitude: 146° strike, 84° dip, 236° dip direction) observed on a subhorizontal surface. A pencil ~18 cm long is shown for scale. Insets: stereoplots of Y- and P-planes. Location: outcrop section in Jasai village area, north of the Jasai railway station; near L3 in figure 1*A*. A color version of this figure is available online.

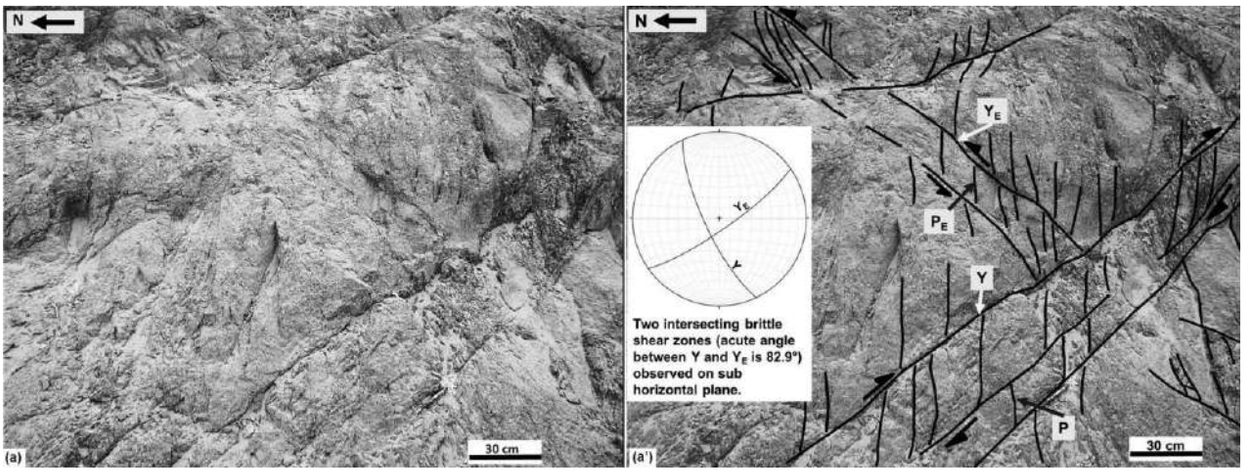

Figure 10. Uninterpreted (*a*) and interpreted (*a*′) photographs of crosscutting brittle shear trending NW and NE, with well-developed P-plane (attitude: 105° strike, 64° dip, 195° dip direction), P_E-plane (attitude: 255° strike, 80° dip, 165° dip direction), Y-plane (attitude: 338° strike, 76° dip, 248° dip direction), and Y_E-plane (attitude: 235° strike, 85° dip, 145° dip direction), observed on a subhorizontal surface of Malani granite terrain. The NW-trending brittle shear, the P- and the Y-planes, cut across the NE-trending brittle shear planes, P_E and Y_E. The angle between the Y- and Y_E-planes is 82.9°, as shown in stereonet plot (*inset*). A pen ~16 cm long is shown for scale. Location: granitic outcrop of the Malani Igneous Suite, NW of Dhorimana village; near L4 in figure 1*A*. A color version of this figure is available online.

major NW-trending Y-plane (dextral shear) crosscuts the orthogonal Y_E-plane (sinistral shear), observed in two outcrops. Hence, the NW-trending Y-plane is younger. A ~10–15-cm-thick melanocratic dike intrudes the NW-trending Y-plane (fig. A7). The NW-trending brittle top-to-SW (up) shear is also seen on a nearly vertical section (fig. 11). A number of slickensides are identified along this fault, indicating that it is reverse-dip-slip (figs. 11, 12*b*). Most of the slickensides/mineral lineation on different fault planes has 75°–90° rake, which indicates dominantly dip-slip movement. A few slickensides with 2°–18° rake indicate almost strike-slip movement (fig. 12*c*, 12*d*). Normal dip-slip movement is also observed on some 58°–78°-dipping fault planes, based on slickenside peaks/asymmetric elevation trends (fig. 12*a*). The Y- and P-planes of the brittle shears are often mineralized.

Along the western rift margin of the Barmer basin, the majority of the brittle shear faults (Y-planes) trend nearly NW to NNW, nearly subparallel to, or at a low acute angle with, the older fractures of the MIS. The dip of the normal faults varies, and sometimes the dip directions of the Y-planes are almost opposite. Also, the majority of the dikes in the western segment of the MIS trend nearly NNW (Pandit et al. 1999; Rao et al. 2003), following the Proterozoic rift fracture trends.

Eastern Margin. The Early Cretaceous fluvial sandstone- and siltstone-dominated succession of the Ghaggar-Hakra Formation is exposed throughout the Sarnoo hill area (L5). In the northern part of the Sarnoo hill area, the lowermost unit of the Ghaggar-Hakra Formation unconformably overlies (figs. 13, A8) or, at places, cuts/truncates (fig. 13) older basaltic rock. The lower unit of the Ghaggar-Hakra Formation, exposed along the unconformity, consists of basal conglomerates overlain by reddish sandstones.

A set of SW-/WSW-trending listric normal faults (fig. 14) are seen in the lowermost sandstone and siltstone unit in NW-SE outcrop cross section (attitude: 255° strike, 35° dip, 165° dip direction). Sandstone beds that dip 11°–15° toward the south/SE are slipped across these listric faults, depicting synthetic relay, with a ~1-dm throw. These listric faults might originate from NW-SE extension during the Mesozoic, and their presence in the lower siltstone-sandstone unit possibly indicates synsedimentary deformation within the Ghaggar-Hakra Formation. Such a small throw indicates prevalence of low strain during deposition of the Ghaggar-Hakra Formation. It also indicates that this siltstone-sandstone unit possesses the competency contrast required for the listricity of the normal faults (Bally et al. 1981; Shelton 1984).

Sandstones of the Early Cretaceous Ghaggar-Hakra Formation reveal that minerals altered and Fe oxide cemented at many places. Y- and P- brittle shear planes are observed within both the sandstone and the basaltic rock body (fig. 15). The majority of the faults trend NE; however, there are a considerable proportion of orthogonal faults as well (pole plots in

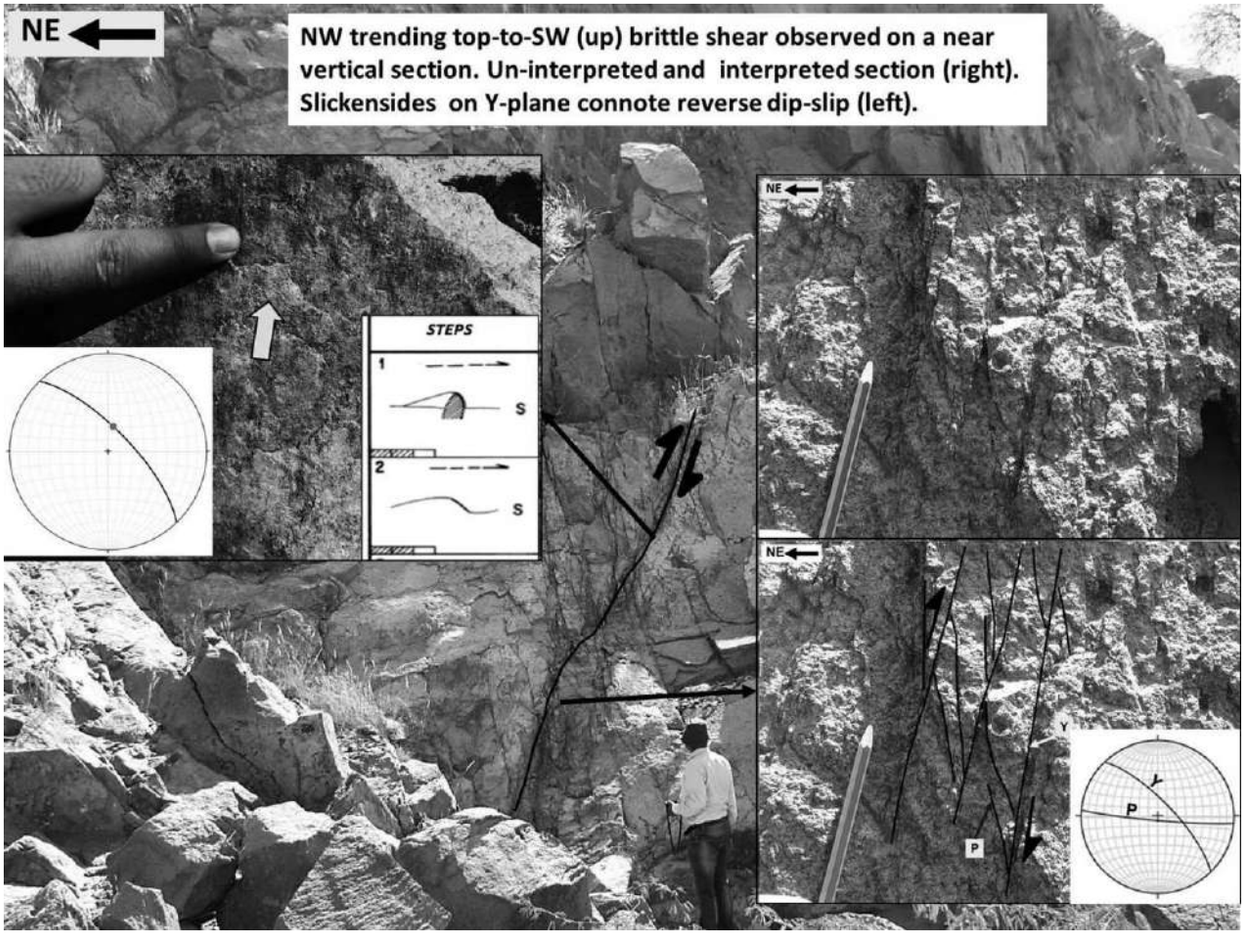

Figure 11. NW-trending large brittle shear feature observed on a subvertical section associated with a Y-plane (attitude: 316° strike, 74° dip, 46° dip direction) and a P-plane (attitude: 95° strike, 86° dip, 185° dip direction). S. Dasgupta (height: 173 cm) is shown for scale. *Right inset*: uninterpreted (*top*) and interpreted (*bottom*) close-ups of the NW-trending brittle shear, with a top-to-SW (up) slip; part of a pencil (~13 cm) is shown for scale; *subinset*: stereoplot of Y- and P-planes. *Left inset*: slickenside associated with stepped feature indicating upward movement (rake: 78°) of the hanging wall; *right subinset*: examples of step slickensides from figure 1 of Doblas (1998); *left subinset*: stereoplot of the fault plane and slickenside. Both of these feature (Y- and P-planes and slickenside) confirm a reverse slip. Location: granitic outcrop of the Malani Igneous Suite NW of Dhorimana village; near L4 in figure 1*A*. A color version of this figure is available online.

fig. 13). Two sets of fractures, trending NW and NE, are also seen at many places in the sandstone body, especially in the eastern part of the hill area.

South-southwest (195°–200°)-trending Y-planes with top-to-south/SSW shear are identified within the older basalt body underlying the Ghaggar-Hakra Formation (fig. A8). A dike trending ~240°–250° obliquely crosscuts the Y-plane (fig. A8). Here a dike truncates a set of P-planes. The dike terminates abruptly against the overlying unconformity (fig. A8). No brittle shear features are seen within the dike. Cross fractures, possibly cooling joints, do exist.

Dextral brittle shear Y-planes trending SW (Y-plane attitude: 220° strike, 57° dip, 310° dip direction; P-plane attitude: 240° strike, 64° dip, 330° dip direction) are identified within basalt, along with a ~20–40-cm-thick fault gouge in a subvertical section (fig. 15). Such a fault can be called a "gouge fault" (Fossen 2016). In the lower part of this reverse fault, a slickenside with 82° pitch connotes dip-slip movement. Such SW-trending reverse faults with nearly top-to-south shear are also observed in the adjacent/overlying lower Cretaceous Sarnoo sandstones. At many places in the western part of the Sarnoo hill area, brittle shear sense is obscured, since these faults/fault zones are characterized by breccias consisting of a knobbly texture associated with clay mineralization and alteration, as described by Taylor (2009) from another terrain.

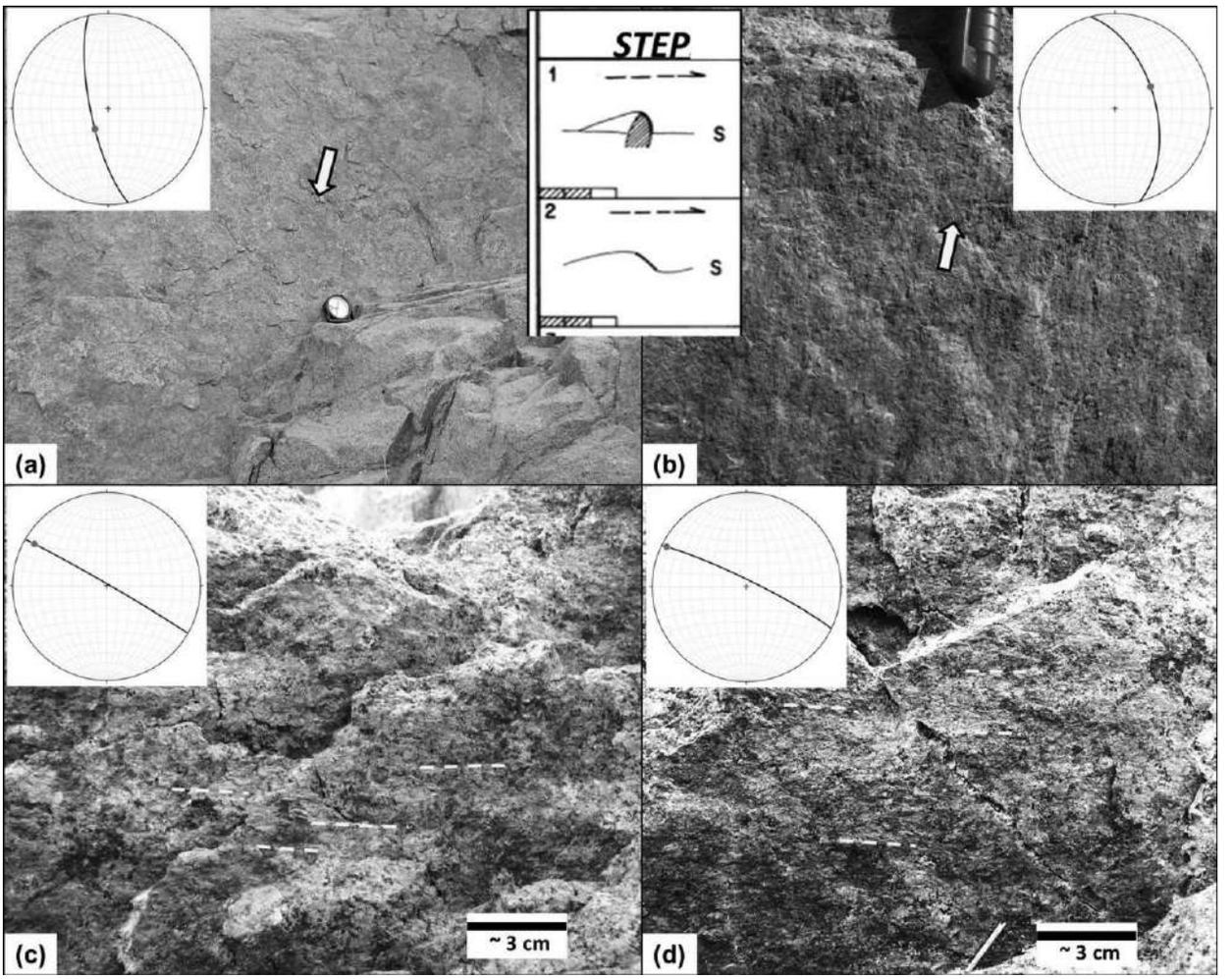

Figure 12. Slickenside features observed on NW- and NE-trending fault surfaces. *a*, Fault surface with slickensides having step-like elevations (rake: ~76°), depicting normal dip-slip movement (attitude: 168° strike, 75° dip, 258° dip direction). A clinometer 8 cm in diameter is shown for scale. *b*, Fault surface with slickensides having step-like elevations (rake: ~80°), depicting reverse-dip-slip movement (attitude: 165° strike, 55° dip, 75° dip direction). Part of a pen cap (~2.7 cm) is shown for scale. *Inset between* a *and* b: examples of step slickensides from figure 1 of Doblas (1998). *c, d*, SE-trending (118°) vertical fault surface with slickenside striations (rake: ~2°–8°), depicting a strike-slip movement. Stereoplots of the fault planes and slickenside features are shown in the insets of the respective panels. Location: granitic outcrop of the Malani Igneous Suite NW of Dhorimana village; near L4 in figure 1*A*. A color version of this figure is available online.

West-southwest-trending faults truncate the SW-trending reverse faults at places (fig. 16). At the eastern part of the hill section, a prominent synsedimentary growth section is observed along the WSW-trending normal fault in the uppermost sandstone unit: the Nosar Sandstone. The Nosar Sandstone thickens adjacent to the WSW-trending normal fault, indicating synsedimentary growth of the sandstone unit associated with fault movement (fig. 16). This WSW-trending normal fault consists of a ~70–100-cm-thick fault gouge. Brittle shear Y- and P-planes of similar trend are also seen within the fault gouge. Y-and P-planes within the fault gouge of same attitude as the fault zone have previously been reported from elsewhere (Mukherjee 2013*b*).

At places, the Nosar Sandstone and the underlying siltstone unit are brittle-sheared, as revealed by Y- and P-planes. The Y-planes trend SW (225°–250°). These are reverse faults with top-to-south shear. Basaltic intrusions occupy these Y- and P-planes within sandstones and siltstones (fig. 17). The basalt veins, at places, also occur as sills and possibly link genetically with the precursor-of-Deccan volcanism. Basalt intruded along Y- and P-planes, presumably

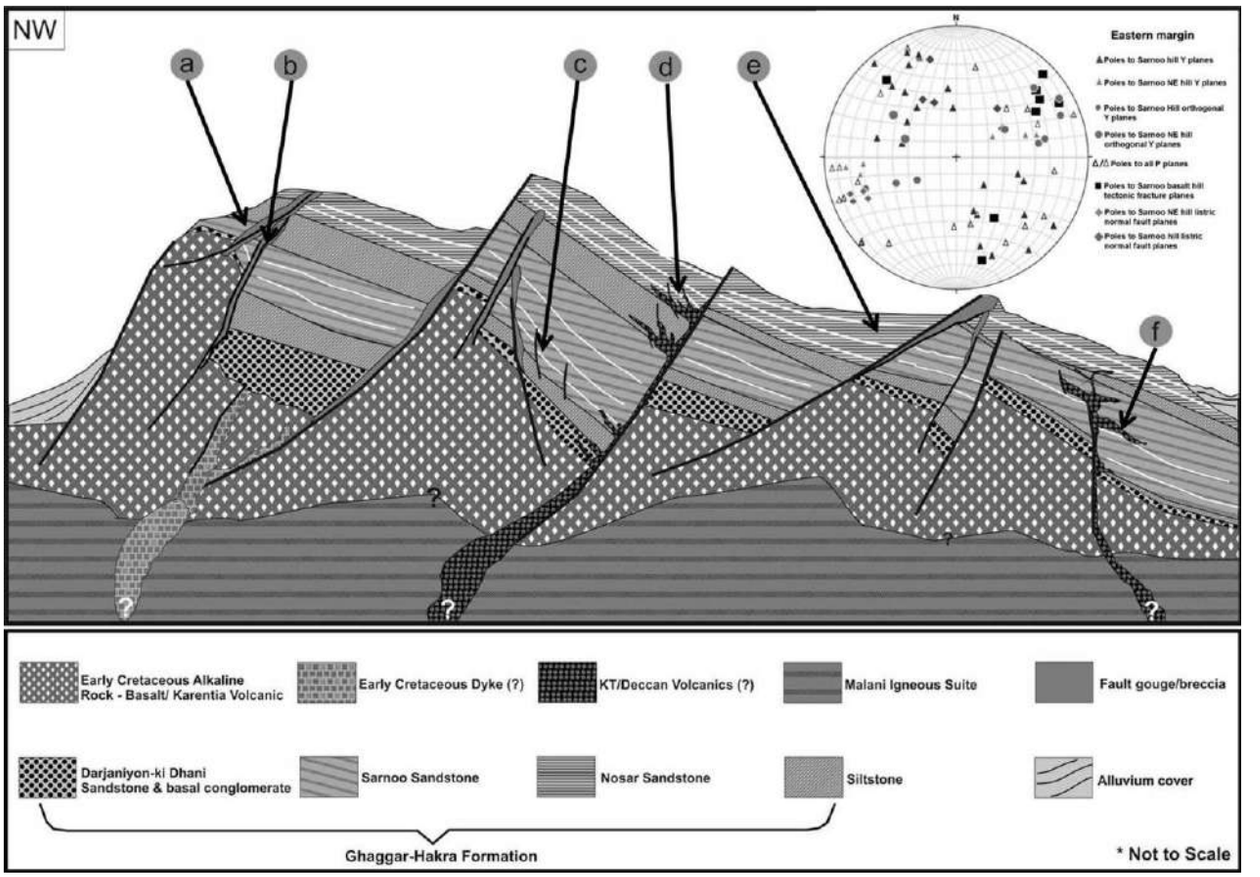

Figure 13. Schematic geological cross section (not to scale) trending SE across the Sarnu/Sarnoo hill area outcrop. Key deformational events in the Sarnu/Sarnoo hill area: large fault gouge section (a); reverse fault often associated with fault gouge and truncation of Ghaggar-Hakra sedimentary strata against older Early Cretaceous volcanics (b; fig. 15); listric normal faults within the lower sandstone-siltstone unit of the Ghaggar-Hakra Formation (c; fig. 14); Deccan-equivalent basaltic flow intruding along the older brittle shears (d; fig. 17); prominent synsedimentary growth feature of the younger sandstone body of the Ghaggar-Hakra Formation along the ENE-trending normal fault (e; fig. 16); and Deccan-equivalent basalt intruding the Ghaggar-Hakra Formation as a sill (f; figs. 19, A10, the latter available online). *Inset*, stereoplot of Y- (solid points) and P- (open points) planes of NE- and NW-trending brittle shear faults identified along the eastern rift shoulder (Barmer basin) in outcrops around the Sarnu/Sarnoo village area. Several orthogonal NW-trending faults are present. A color version of this figure is available online.

after those two sets of planes developed. Some of the WSW-trending faults show dip-slip movement, as deduced from the slickenside stepped elevation developed on the fault-plane surface with 78° pitch (fig. 18).

At places in the Sarnoo hill area, ~1–2-m-long SE/SSE-trending brittle shear Y-planes of mostly reverse faults (fig. A9) are observed on subvertical rock sections within the Ghaggar-Hakra Formation sandstone. The sense of shear is dominantly top to nearly east (up), with a few showing top to nearly west (down) shear sense. In two cases, SE-trending normal faults ≥3 m long were also documented (fig. A9), which could possibly indicate the main phase of rifting of the Barmer basin.

We also studied an exposure ~500–600 m NE of the Sarnoo hill area (L5) beside State Highway 16/National Highway 115, where the lower part of the Ghaggar-Hakra Formation is exposed (Bladon et al. 2014) with basalts as sills. In the lower part of the exposure, sandstones and siltstones are reddish and are baked at many places by intrusion. A number of normal and reverse faults presumably dissected the NW-facing side of the NE/ENE-trending hillock. The SSE-trending reverse faults are present below the basalt sill layer and consist of brittle shear Y- and P-planes. These reverse faults occur as conjugate sets with opposite vergence (fig. A10), without cutting each other. The basalt sill body, at places, is partially displaced in the form of a drape fold by the under-

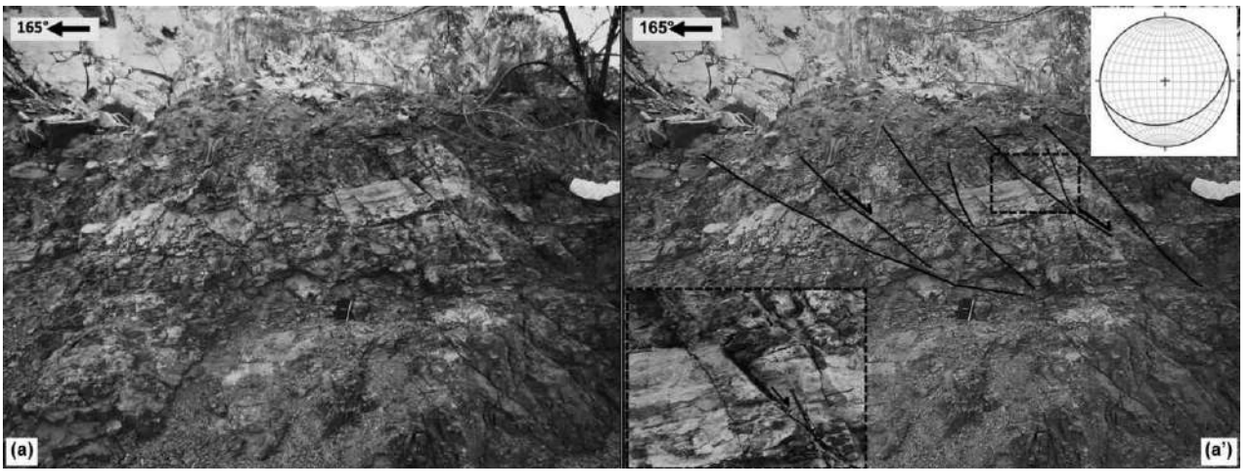

Figure 14. Uninterpreted (*a*) and interpreted (*a′*) photographs of listric normal faults (attitude: 255° strike, 35° and varying dip, 165° dip direction) trending SW to WSW in sandstone-siltstone unit of the lower Ghaggar-Hakra Formation, observed on a subvertical section. Throw ranges from a few to 20–30 cm. A field notebook ~14 cm long is shown for scale. *Inset*, stereoplot of the fault plane. Location: NW part of the Sarnu/Sarnoo hill area; near L5 in figure 1*A*. A color version of this figure is available online.

lying fault, resulting in a small-scale monocline (fig. 19*a*, 19*a′*). At places, the overlying sill, too, is brittle-sheared. At one outcrop, SE-trending conjugate normal faults slipped the basalt sill, giving a small-scale full graben (fig. 19*b*, 19*b′*). At some places, these normal faults are slightly listric. The listricity probably arises because of the competency contrast across the layered lithology of the rock body. These observations indicate that the SE-trending faults postdated basalt intrusion, probably during the main phase of Barmer rifting in the early Tertiary or at the K-T boundary.

Outcrops farther east and SE of the Sarnoo hill area, ~800 m–1.2 km from Sarnoo village (L5), consist of massive basalts. They consist of well-developed plagioclase laths depicting near-linear lava flow (fig. A11*a*). No major shear developed in these basalt outcrops. At one location, near the base of a basalt hill, two

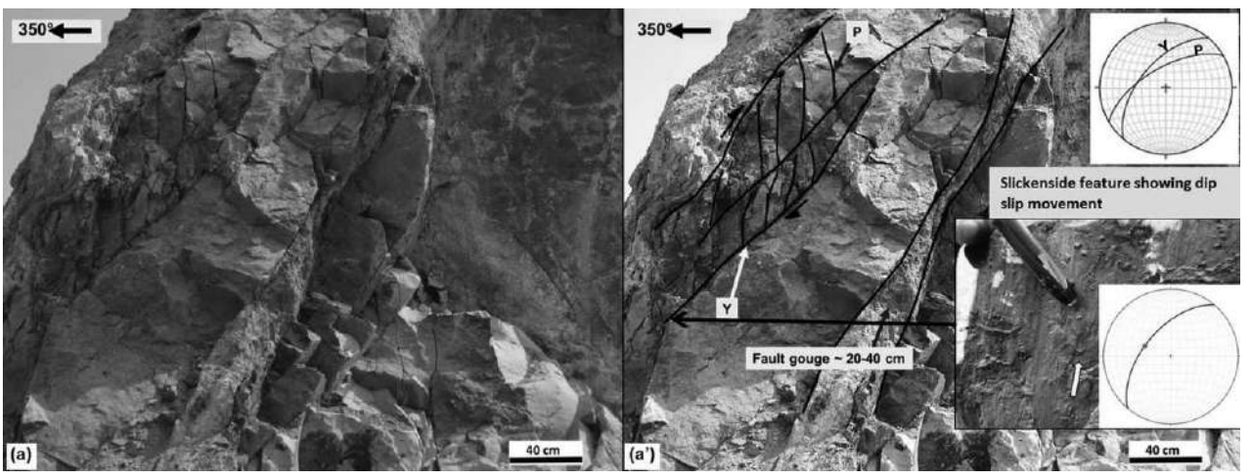

Figure 15. Uninterpreted (*a*) and interpreted (*a′*) photographs of the lower Ghaggar-Hakra Formation, depicting a top-to-SSE brittle shear feature associated with a Y-plane (attitude: 220° strike, 57° dip, 310° dip direction) and a P-plane (attitude: 240° strike, 64° dip, 330° dip direction) in a lower (older) basalt unit; there is a 20–40-cm-thick fault gouge along the Y-plane. *Top inset*, stereoplot of Y- and P-planes. *Bottom inset*, slickenside striations (rake: 82°) on exposed Y-planes indicate reverse dip-slip movement. Part of a pen (~4 cm) is shown for scale. *Subinset*, stereoplot of the Y-plane associated with the slickenside feature. Location: NW part of the Sarnu/Sarnoo hill area; near L5 in figure 1*A*. A color version of this figure is available online.

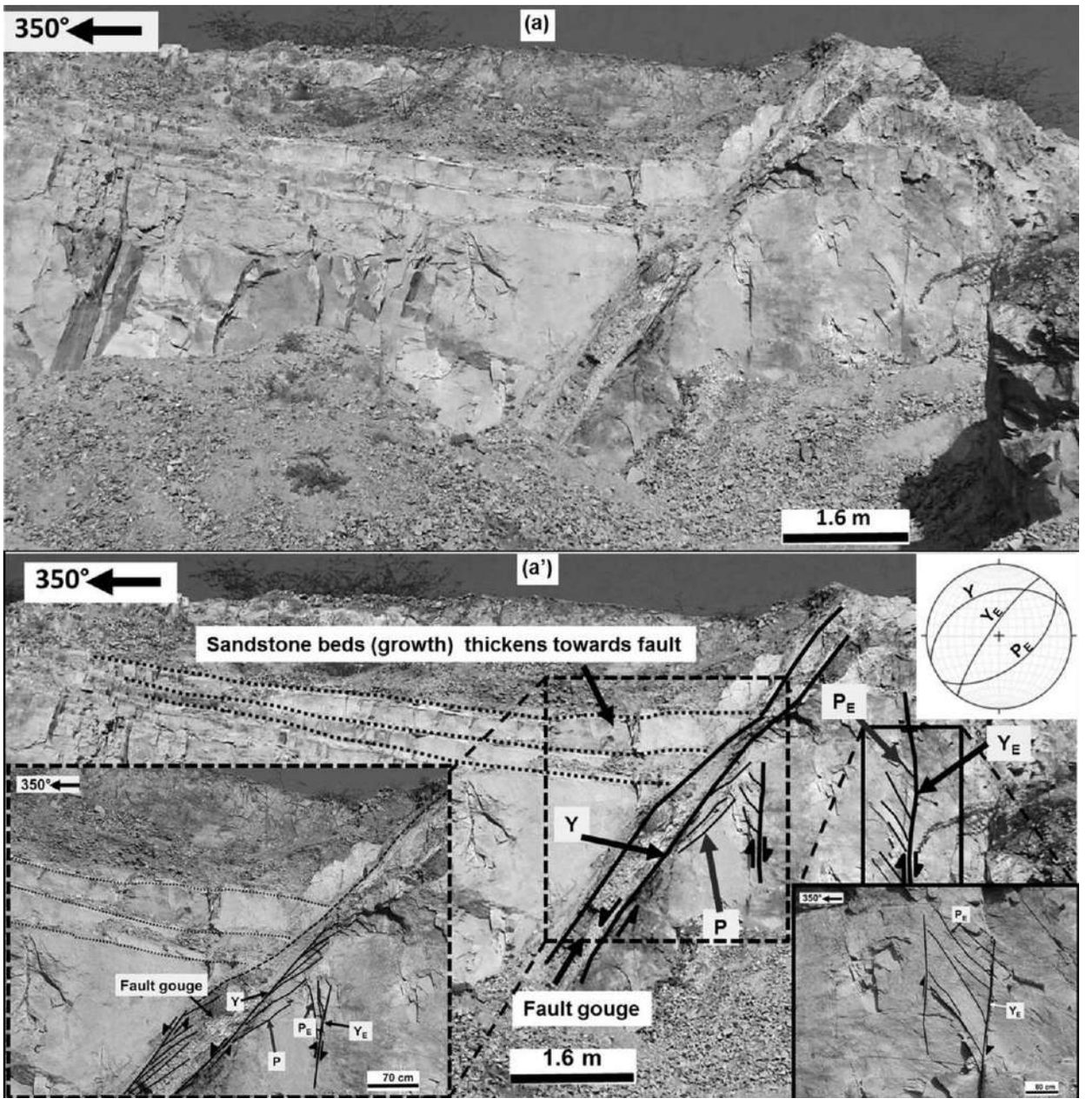

Figure 16. Uninterpreted (*a*) and interpreted (*a*′) photographs of upper part of the Ghaggar-Hakra Formation, depicting that the WSW-trending normal fault, associated with a Y-plane (attitude: 250° strike, 38° dip, 340° dip direction) and a P-plane (not measurable), has cut across the older SW-trending brittle shear faults with a Y_E-plane (attitude: 215° strike, 79° dip, 305° dip direction) and a P_E-plane (attitude: 232° strike, 53° dip, 142° dip direction). Distinct synsedimentary growth of the sandstone body is observed along the normal fault in the vertical section. This WSW-trending normal fault is also associated with a ~50–120-cm-thick fault gouge, which also consists of P-planes. *Inset*: Stereoplot of Y-, Y_E-, and P_E-planes. Location: eastern part of the Sarnu/Sarnoo hill area; near L5 in figure 1*A*. A color version of this figure is available online.

sets of fractures are identified. The dominant one trends SE (~130°–150°) and the other SW (~228°; fig. A11*b*).

Devikot-Fatehgarh Ridge. We studied (1) the uplifted ridge on the eastern side of National Highway 15 (NH-15) and (2) the ridge section on the western side of this highway. The main rock types are cross-bedded sandstones, overlain by a discrete thin layer of calcrete (fig. 20), followed by a volcanic ash bed and finally silty mudstone at the top. The

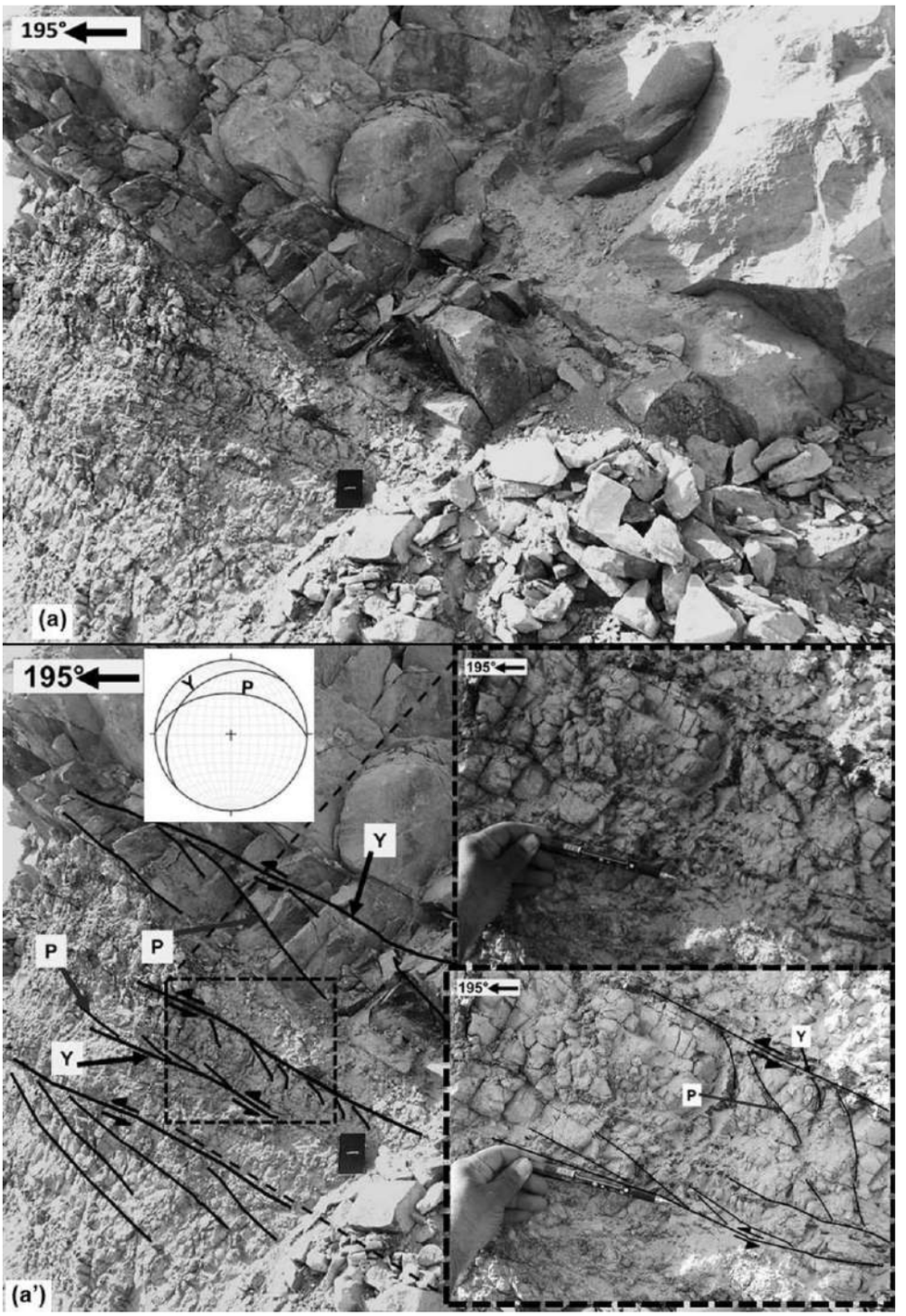

Figure 17. Uninterpreted (*a*) and interpreted (*a*′) images of the upper portion of the Ghaggar-Hakra Formation, depicting a SW-trending brittle shear fault within sandstone and underlying siltstone units, from a near-vertical section. A thin basaltic flow occupied the Y-plane (attitude: 225° strike, 24° dip, 315° dip direction) and the P-plane (attitude: 92° strike, 44° dip, 02° dip direction) within the siltstone and partly the sandstone unit. A field notebook ~14 cm long is shown for scale. *Right insets*, close-ups depicting the basaltic flow occupying Y- and P-planes. A pen ~16 cm long is shown for scale. *Left inset*, stereoplot of Y- and P-planes. Location: eastern part of the Sarnu/Sarnoo hill area; near L5 in figure 1*A*. A color version of this figure is available online.

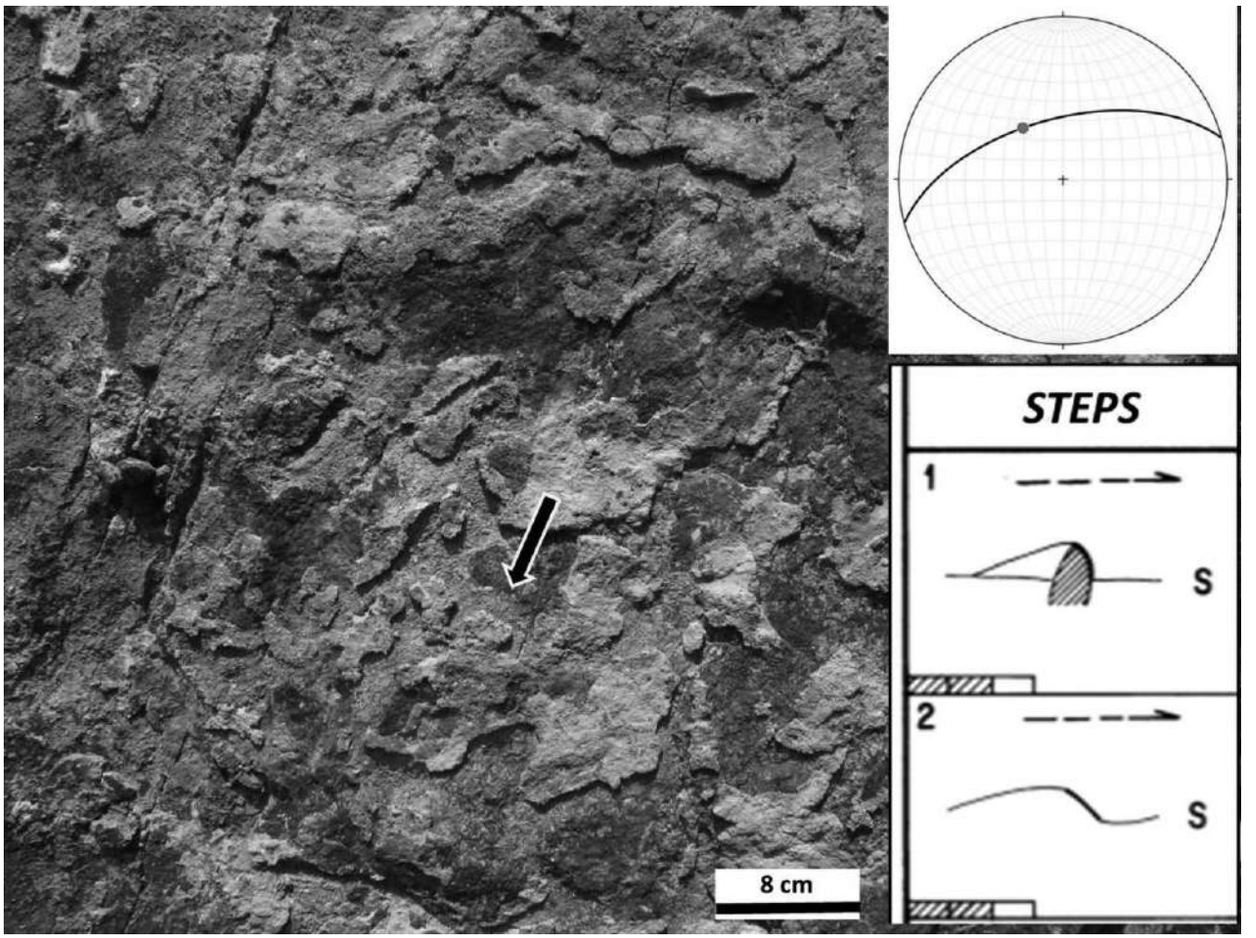

Figure 18. Slickenside feature along the WSW-trending fault (attitude: 255° strike, 59° dip, 345° dip direction), depicting step-like elevations (pitch: 78°) indicating a normal dip-slip movement with the hanging-wall block going down. *Bottom right*, examples of step slickensides from figure 1 of Doblas (1998). *Top right*, stereonet plot of the fault plane along with the slickenside feature. Location: eastern part of the Sarnu/Sarnoo hill area; near L5 in figure 1*A*. A color version of this figure is available online.

purple-brown volcanic ash bed is ~15–30 cm thick variably and occasionally is associated with dark, fine-grained porcellanite. The sandstone unit is dominantly cross bedded. This is evidently a fluvial channel deposit, as suggested by the erosive concave-up lower-bound surface (fig. 20*a*). The sandstone body was later cut by tectonic fractures, and these often contain carbonate precipitates (fig. 20*b*). At places above the cross-bedded sandstone unit, a parallel laminated finer sandstone body is present, with occasional thin calcrete layers (fig. 20*c*, 20*d*).

The Devikot-Fatehgarh Ridge extends up to 20–30 km, with an uplifted sedimentary sequence that dips 20°–45° toward the south or SE. No brittle shear features exist. This entire uplifted fault scarp section manifests itself as nearly NE-trending disconnected hillocks. This indicates that this reactivated high is not the result of a well-established full-length fault (inset *i* of fig. 21). It can be better defined as segmented fault system (Fossen 2016) that is linked by relay structures (Peacock and Sanderson 1991; Fossen and Rotevatn 2016). This is also evident from the Google Earth Pro satellite imagery (fig. 21). At some places (fig. 21*a*, 21*b*), mainly on the eastern side of NH-15, these relay features can be explained as "synthetic approaching transfer zone," as in Morley et al. (1990). In such areas, the vertical displacement along two adjacent ridges, sloping in same direction, reduces as they approach each other. This is observed in the field as well as through the Google imagery (fig. 21*a*, 21*b*).

All along the linear extent of the uplifted ridges, the relay structures are mostly soft-linked by relay ramps (reviewed in Fossen and Rotevatn 2016). A few hard-linked relay structures associated with a set of tectonic fractures exist in the outcrops. These tec-

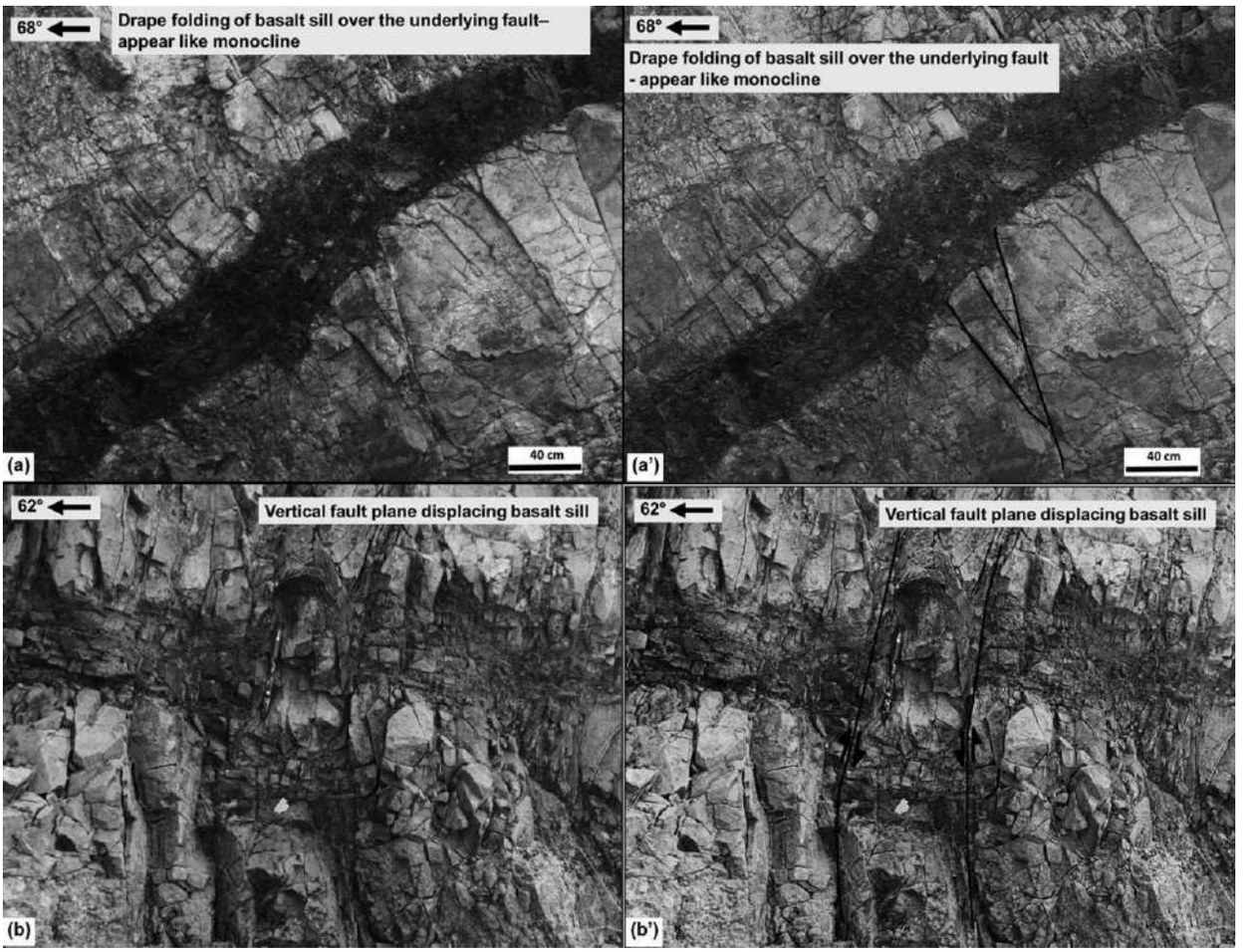

Figure 19. Uninterpreted (*a*, *b*) and interpreted (*a′*, *b′*) images from near a vertical section of the lower Ghaggar-Hakra Formation show brittle deformation within the basalt sill body. *a*, *a′*, Listric brittle plane associated with fractures (attitude: 173° strike, 73° dip, 83° dip direction) below the basalt sill has deformed the sill body, thereby forming a drape fold or monocline. *b*, *b′*, A set of normal faults (attitude: 160° strike, 64° dip, 70° dip direction) displaced the basalt sill layer, producing a small-scale full graben. A pen ~16 cm long is shown for scale. Location: west-facing outcrop hillock, 600 m NE of Sarnu/Sarnoo village; near L5 plotted in figure 1*A*. A color version of this figure is available online.

tonic fractures normally have higher dip (>45°) and trend nearly SE/WSW (inset *ii* of fig. 21). The SW/WSW-trending fracture sets may be linked to the main reactivated fault associated with linearly dispersed ridges, while their nearly orthogonal sets are likely to be related to the breached relay ramps (Fossen and Rotevatn 2016) or transfer fault geometries. These orthogonal sets of tectonic fracture are observed in the lower sandstone unit as well as in the volcanic ash bed. However, discrete calcrete layers are unfractured. At many places, the fracture surfaces within the sandstone body are coated with calcrete, indicating fluid flow (fig. 20*b*; Caine et al. 1996). West of NH-15, the volcanic ash beds are slipped by brittle faults(?) showing n-type drag (review in Mukherjee 2014; also see Mukherjee 2011; Mukherjee and Koyi 2009) trending south, as observed in a subhorizontal section (fig. A12). This fracture could be associated with a transfer fault or a breached relay structure having a sinistral slip. Subsurface evidence through geophysical study can confirm the presence of a fault.

Weathering-related fracture planes in granites and volcanic ash resembled P-planes. These were not considered to have brittle shear sense, since such curved planes were not found to be bound by another set of planes supposed to be Y-planes (fig. A13*a*, A13*b*).

Discussion

Stereoplots of poles of planes measured in the field from the eastern (Sarnoo hill area; fig. 13) and west-

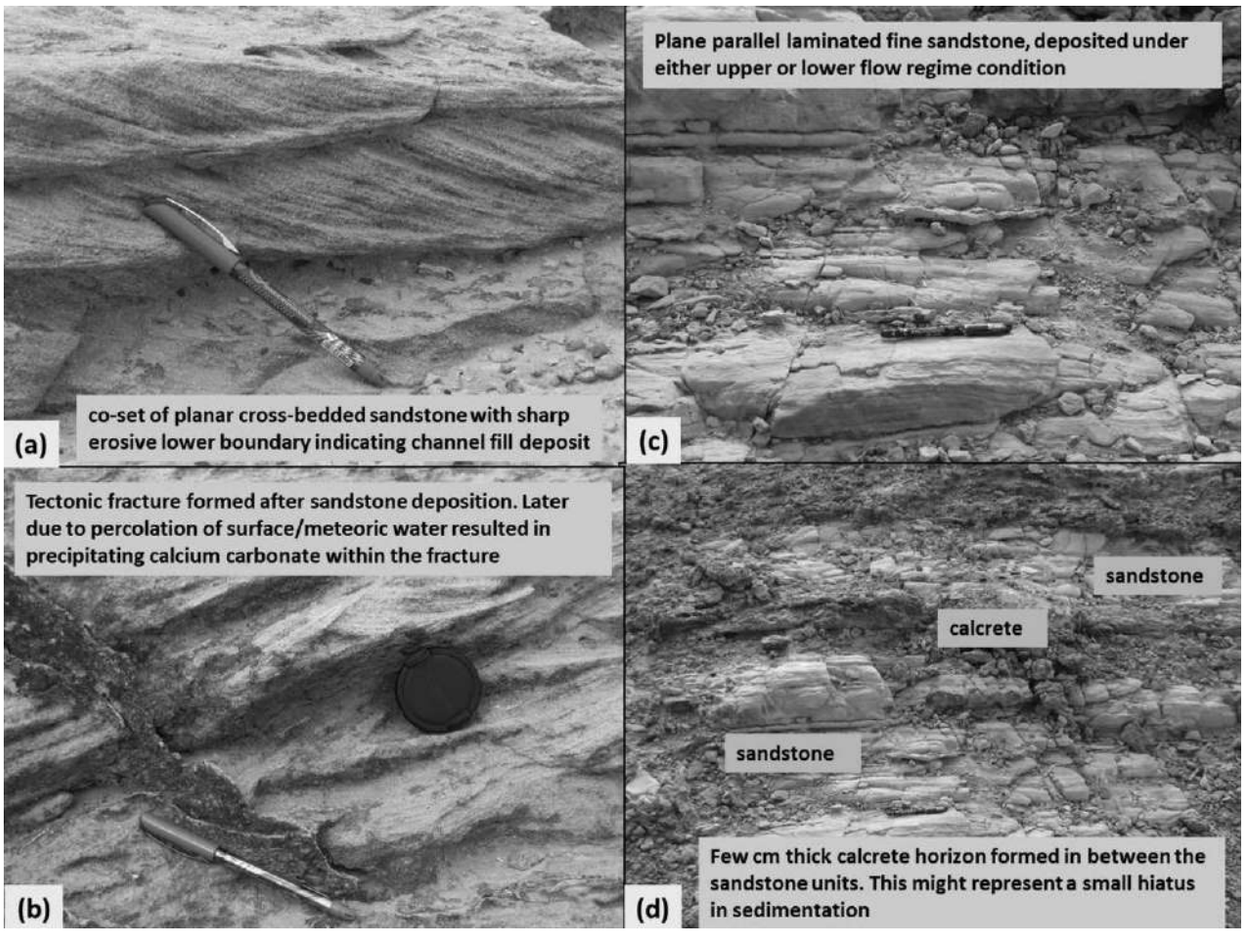

Figure 20. Different types of depositional systems of the sandstone body in the Fatehgarh Formation exposed near Bariyada along the Devikot-Fatehgarh ridge. *a*, Co-set of planar cross-bedded sandstone. These sets were truncated by the overlying ones. The lower boundary is sharp, erosive, and concave-up. The set thins upward. Channel deposition is indicated (Elliott 1978; Collinson and Thompson 1984). *b*, Fracturing after sandstone lithified. Later, percolating water precipitated carbonates and probably kaolinites within these fractures. *c*, Plane-parallel laminated fine sandstone, deposited under either an upper or a lower flow regime. *d*, Few-centimeters-thick calcrete horizon within sandstone units, possibly representing a hiatus in sedimentation. The hiatus was after the sandy bar formed. The calcrete horizon formed meanwhile. A pen ~16 cm long and a camera lens cover ~6 cm in diameter are shown for scale. Location: near L6 in figure 1*A*. A color version of this figure is available online.

ern (Barmer area, Dhorimana, and Jasai; fig. 4) margins show distinct variation of the fault trends. In the western margin of the rift shoulder, the majority of the faults strike NW and dip nearly SW. The NE-striking orthogonal faults are fewer. Most of these orthogonal faults are dominantly strike-slip, as identified from field study. Hence, these orthogonal faults mainly act as stress transfer faults. Because of continuous extension during the main phase of Barmer rifting, strain localized at the rift shoulders located ~10–15 km farther west of rift margin (fig. 1*A*).

In the Sarnoo hill area of the eastern-margin rift shoulder, most of the faults trend NE and dip toward the SE. These are probably related to transtension during the Early Cretaceous (Bladon et al. 2015). This transtension is due to initiation of strike-slip movement between India and Madagascar (Misra et al. 2014, 2015; Gaina et al. 2015; Misra and Mukherjee 2015, 2017). However, unlike the western margin, this area has several antithetic faults.

The NE-trending faults vary considerably in strike, from SSW to WSW. At one location, a WSW-trending normal fault truncates the SW-trending faults (Y-planes). Moreover, synsedimentary deformation of the Early Cretaceous sandstone, having low strain, is seen along the SW- to WSW-trending normal faults at two locations. This was missed by Bladon et al. (2014). Whether this indicates a clockwise rotation

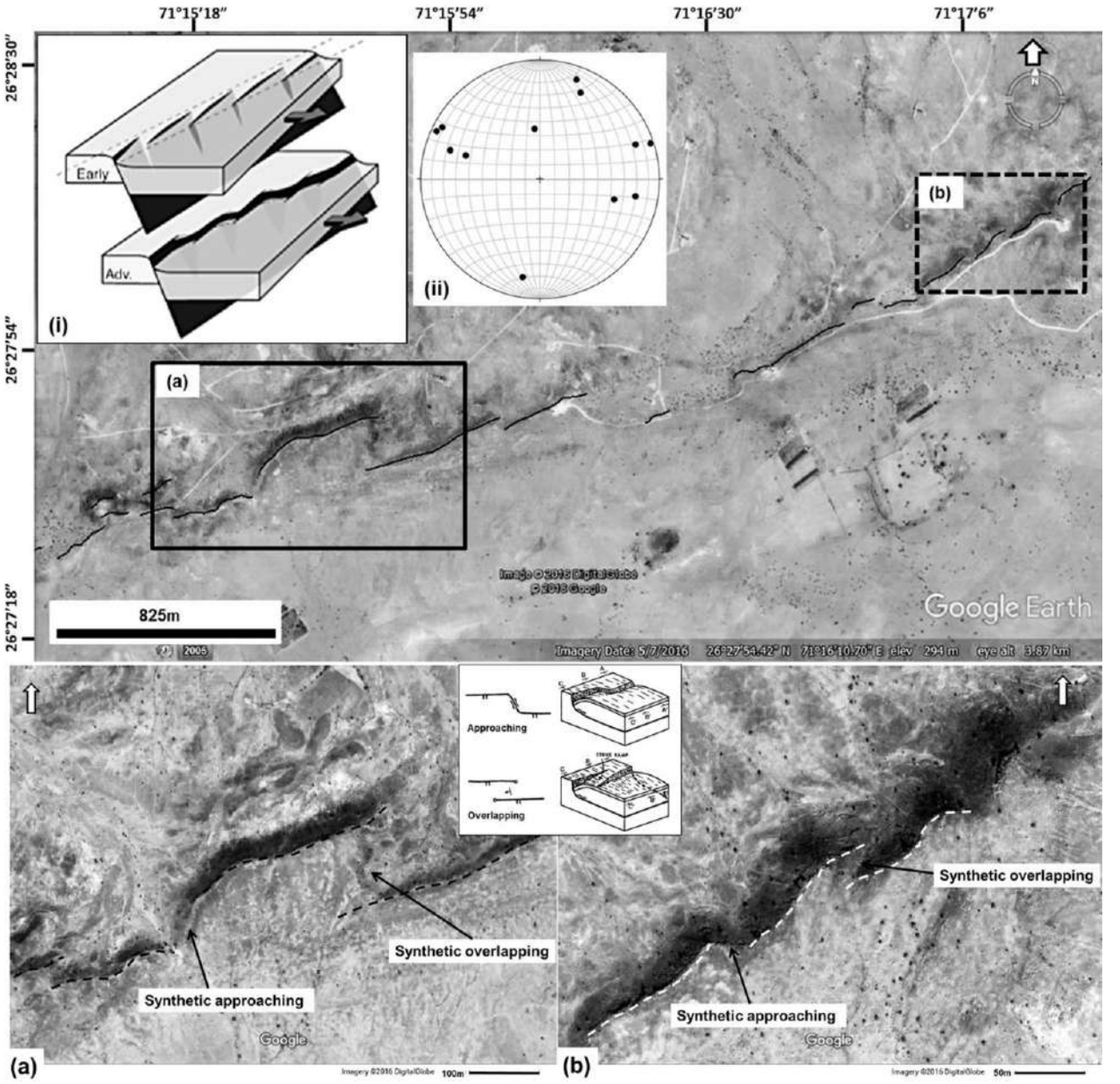

Figure 21. Segmented fault system associated with relay structures along the NE-trending Devikot-Fatehgarh ridge, as observed from Google Earth Pro satellite imagery. *Inset i*, segmented fault systems may link up in the advanced stage, influenced by preexisting basement structures (fig. 4*c* in Fossen and Rotevatn 2016). *Inset ii*, pole positions of fracture trends along the Devikot-Fatehgarh ridge. Location: ~115 km NNE of Barmer town, east of National Highway 15; near L6 in figure 1*A*. *a*, *b*, Relay structures, observed from Google Earth Pro satellite imagery. *a*, Relay structure associated with synthetic overlapping fault system at right and possibly hard-linked relay ramp at left. *b*, Set of relay structures, central part: synthetic overlapping relay ramp and left-breached or hard-linked synthetic approaching relay structure. *Inset*, examples of synthetic transfer zones in figure 4*a*, 4*b* of Morley et al. (1990). Location: ~115 km NNE of Barmer town, 10–15 km east of National Highway 15; near L6 in figure 1*A*. A color version of this figure is available online.

of the stress axes during the Early Cretaceous NW-SE extension can be addressed by paleostress analyses.

Northwest-striking orthogonal faults are more abundant in the Sarnoo hill area, in the eastern margin. This indicates that the main phase of Barmer rifting, which initiated in the Late Cretaceous and continued though the Paleocene, affected considerably the fault morphology on either side of the rift margin. This is also evident from (1) the usual SE trend of the tectonic fractures observed in the basalt

hill outcrop, about 1 km SE of the Sarnoo hill area, and (2) the SE-trending normal faults that have displaced basalt sills in the NE Sarnoo hill area. This also indicates that the precursor magmatism of the Deccan event intruded the eastern margin of Barmer rift basin. Evidence of the Deccan Trap precursor has been reported by some authors from the Sarnoo-Travidar-Dandali areas (Roy 2003; Vijayan et al. 2015).

Conjugate brittle faults were documented from the Dhorimana, Jasai, Genhoo, and NE Sarnoo outcrops (figs. 8, 10, A6, A10). Of these, a crosscutting relation is seen only in the Genhoo and Dhorimana areas (figs. 8, 10). The acute angles between these conjugate sets of faults range 64°–83°. Although in most cases these conjugate faults are linked to separate extensional events—NW extension in the Early Cretaceous and NE extension during the Late Cretaceous to Paleocene—whether they developed simultaneously would be interesting to investigate.

Classical Andersonian fault systems follow the Mohr-Coulomb fracture criterion and form by coaxial pure shear (Anderson 1905; Healy et al. 2015), leading to coeval conjugate faulting. The maximum principal stress (σ_1) is the acute bisector of the angle between the conjugate faults. The σ_1 makes a 30° angle to both the fault planes, whereas the minimum principal stress axis (σ_3) is the obtuse bisector of the conjugate faults. The intermediate principal stress (σ_2) is the line of intersection between the conjugate faults, which is horizontal. A deviation from such conditions is a non-Andersonian faulting. In such a case, σ_2 is not parallel to the intersection of the fault sets but rather lies obliquely. An example of non-Andersonian faulting is that produced by brittle shear in a simple shear regime under noncoaxial deformation (Yin and Taylor 2008). Such shears produce R_1 and R_2 Riedel shears and subsequently the primary P-shear. The conjugate brittle shear faults observed in the granite hill in the Dhorimana area and that from the Sarnoo hill area exemplify non-Andersonian faulting. This is because the acute angle between the two conjugate faults exceeds considerably the Andersonian 60°. The Barmer rift being filled up by layer sedimentary rocks, the applied tectonic stress varied, presumably through those layers (e.g., Roche and van der Baan 2017). This possibly produced non-Andersonian faulting within the basin. Anisotropy within a rock body also leads to non-Andersonian faulting (Sibson et al. 1988; Yin and Ranalli 1992).

A number of slickenside features identified from the different outcrops in the western margin indicate that the NW- to NNW-trending faults are dominantly dip-slip. On the other hand, the WNW- and NE-tending faults are mainly strike-slip (fig. 12). The Proterozoic rift fractures of the MIS probably favored the main Barmer rifting. These rift fractures, trending nearly north, are at a high acute angle to the NE-SW extension (fig. 1*Biii*). In some cases, they tend to be nearly perpendicular to the extension direction (fig. 1*Bi*). Thus, we postulate that the preexisting anisotropy (discrete) related to the MIS rift fractures, as well as the NE-trending Early Cretaceous faults, favored the main phase of Barmer rifting.

The northern margin of the Barmer basin is bounded by the NE/ENE-trending Devikot-Fatehgarh Fault/fault scarp. It consists of a chain of uplifted ridges all along this trend. The isolated ridges interlink by relay/transfer structures (as in Fossen and Rotevatn 2016), along which slip propagated. The gravity anomaly data suggest that the Malani igneous basement is shallow in this area and thus has thin sedimentary cover (Mishra 2011). This initiates the reactivation of preexisting rift fractures, trending NE, under the new NE-SW stress regime.

Toward the easternmost side (fig. 21) and also in the westernmost limit, to some extent, in the northern portion of the Barmer basin, the relay ramps breach, that is, the faults connect as fault tips propagate. This process can be defined as a single-tip breach (Fossen and Rotevatn 2016), which actually describes transfer faults connecting synthetic fault systems (as in Morley et al. 1990; Morley 2002). Interestingly, such relay structures and/or transfer zones are also seen in subsurface fault maps of the Barmer basin (Bladon et al. 2015). Relay structures play a key role in rift fault propagation and thus in synrift sediment distribution and hydrocarbon and hydrothermal fluid migration (Caine and Forster 1999), as well as in entrapment of hydrocarbon. The transfer zones have a close connection with the preexisting basement fractures/weak planes (Morley 1999; Morley et al. 2007). Wider and longer relay structures are easily formed under the influence of preexisting basement fractures. This has been reported from various continental rift basins worldwide (Peacock and Sanderson 1991; Baudon and Cartwright 2008; Misra and Mukherjee 2015; Fossen and Rotevatn 2016).

A number of reverse slips along subvertical faults are observed from field study of the Barmer rift basin: in the Gehnoo, Jasai, and Dhorimana areas (figs. 11, A4, A6) along the western margin, trending NW to NNW, and in the Sarnoo hill area (figs. 15, 16, A10) along the eastern margin, trending NE. The most likely cause of this reverse faulting, as observed from the Barmer rift margin, is isostatic

flexture–related contraction (as in Lewis and Baldridge 1994) along the weak zones in the MIS. The preexisting rift fracture zones within the MIS can be reactivated. The Réunion plume–related alkaline igneous complex present in the Sarnoo hill area and Tavidar along the eastern rift margin is associated with these weak zones (Basu et al. 1993; Raval and Veeraswamy 2000; Roy 2003; Sharma 2007). Another possible cause of reverse faulting in the western margin could be related to far-field ridge-push-related compression (Withjack et al. 1995) during separation of the Seychelles microcontinent from India.

Several neotectonic lineaments in western Rajasthan, India, trend NW to NNW (fig. 1*A*). Some smaller, unnamed ones also trend NE (fig. 1*A*). Some of these lineaments govern recent geomorphic features, such as changing a river course; for example, the Luni River (Bajpai 2004) runs parallel to the NE-trending Luni-Sukri lineament after taking a high-acute-angle turn from its nearly north/NNE-trending course, toward the south of the Barmer basin (fig. 1*A*; fig. 5 of Bakliwal and Wadhawan 2003). Two moderate-intensity earthquakes were reported in 1985 and 1991 about 16 km NW of Barmer town and 50 km SE of Jaisalmer town, respectively (www.earthquaketrack.com; Bakliwal and Wadhawan 2003; Roy 2006). These quakes might be genetically related to one of these lineaments. Reactivation of the NW-trending Konoi/Kanoi fault in the Jaisalmer area was reported in the 1991 earthquake (Joshi et al. 1997; Laul 2000; Bakliwal and Wadhawan 2003). The question arises whether any of these neotectonic lineaments are related to these reverse faults. Study of the fault-plane solution (McKenzie 1969) from earthquake data of the Kutch basin (Chandra 1977; Chung and Gao 1995) depicts a nearly north-trending P-axis. The SH_{max} (σ_1 in Andersonian notation) trends nearly north to NNE (Chandra 1977; Rajendran et al. 1992). Specifically, Abdelaziz et al. (2016) found 25°N to be the direction of the SH_{max} from an undisclosed location in the Raag (Raageshwari) Deep oil field in the Barmer basin, on the basis of image and sonic logs. The P-axis trend obtained from the Kutch earthquake study is nearly perpendicular to the reactivated, nearly ENE trending basin margin faults acting as one of the nodal planes (Chung and Gao 1995). This type of similarity could be drawn for the Fatehgarh-Devikot ridge/Fatehgarh fault in the northern margin of the Barmer basin, which trends NE and has reverse displacement possibly due to the Himalayan orogeny. However, the reverse slip along faults seen within the granite/rhyolite rock bodies in the Dhorimana, Jasai, and Gehnoo hill areas trend NW to NNW and thus would be at an acute angle to the P-axis trend. In addition, there is no uplift of sedimentary cover seen in areas surrounding the granite/rhyolite outcrops. Thus, it seems that these reverse faults in the MIS along the western rift margin of the Barmer basin are independent of Himalayan (neo)tectonics. The Jaisalmer-Barwani lineament (Bakliwal and Wadhawan 2003; Roy 2006) runs along the western rift margin of the Barmer basin (fig. 1*A*). Although no major neotectonic displacement has been reported along the western margin of the Barmer rift basin, a possibility of local stress buildup along this rift margin cannot be ruled out.

Bladon et al. (2014) referred the structural inheritance of the Barmer basin from nearly west/SW-trending faults related to NW extension in the Mesozoic, as identified from the eastern and NE part of the basin and also from the Sarnoo hill area outcrop. We postulate inheritance from both the western and eastern margins from the preexisting (discrete) Proterozoic, nearly north-trending rift fractures of the MIS.

Fault network topology can be used on a subsurface fault map to understand the relative connectivity and to quantify various spatial relations between faults and/or fractures (Sanderson and Nixon 2015; Duffy et al. 2017). The fault geometry evolves temporally, with increasing strain during rifting phases. This changes the topological parameters (nodes and branches between the nodes; Duffy et al. 2017). The measure of connectivity per branch (C_B), a function of counts of different nodes, varies between 0 (no connecting branches) and 2 (maximum connection) for single-phase (low strain) to multiphase extension events (Duffy et al. 2017). Thus, topology can help in the analysis of the different phases of extension, the rotation of stress axes with time, the impact of preexisting structural features, and also fluid migration pathways (Morley and Nixon 2016; Duffy et al. 2017). Since the Barmer rift basin underwent two noncoaxial extension events and is guided by the preexisting structures of the MIS, we presumed that the C_B value may range from ~0.8 to 1.3. Detailed topological analysis on a subsurface seismic data–derived fault map can validate this.

Gombos et al. (1995), Biswas (1987), Pandey and Agrawal (2000), Reeves (2013), and Gaina et al. (2015) reviewed tectonics of western Indian basins. Our work leads to the following synthesis (fig. 22). The Gondwana fragmentation during the Jurassic developed two major Mesozoic basins in western India. These are the Jaisalmer basin of Rajasthan and the Kutch basin of Gujarat. The opening of the Somali basin during the Jurassic produced a shelf-slope system in western Rajasthan, the Jaisalmer basin being a part of this broad shelf. The Lathi

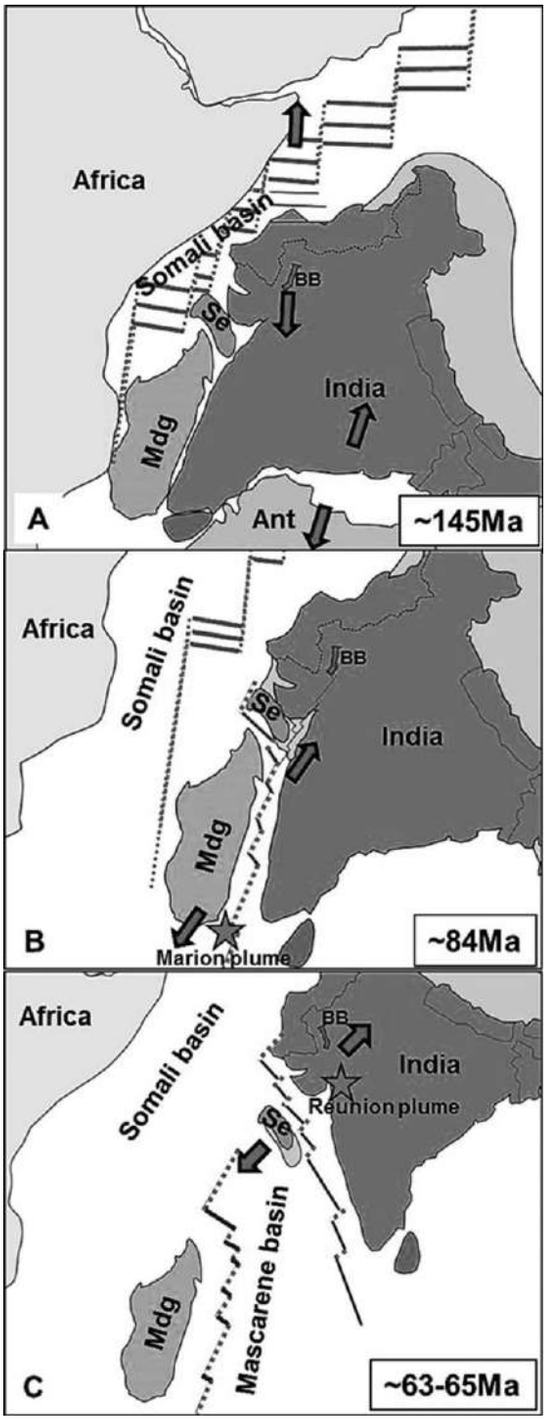

Figure 22. Plate tectonic model (schematic diagram): greater India, Seychelles, and Madagascar with respect to East and NE Africa at different times (after Gibbons et al. 2013; Reeves 2013; Misra et al. 2014; Gaina et al. 2015). *A*, The Somali basin formed at the end of the Jurassic (145 Ma). *B*, Madagascar separated from India-Seychelles in the Late Cretaceous (~84 Ma). *C*, Cretaceous-Paleocene rifting between India and the Seychelles microcontinent. Probable transform fault and spreading centers shown in dashed and solid lines, respectively. Ant = Antarctica; BB = Barmer basin; Mdg = Madagascar; Se = Seychelles micocontinent. Arrows indicate the direction of maximum extension/σ_1/SH_{max}. A color version of this figure is available online.

Formation, reported from Jaisalmer and parts of the Barmer basin, was deposited during this period. This early phase of extension might have resulted in the low-strain present-day NE-trending faults in the Barmer basin that acted as a sweet spot for initiation of transtentional activity in consequence of Madagascar's separation from the Indian plate during the Cretaceous (~88–84 Ma; Storey et al. 1995; Reeves 2013). However, the amount of strain was not intense enough to develop a mature rift basin. This condition was fulfilled during separation of the Seychelles microcontinent in the Maastrichtian, followed by Réunion plume activity that finally separated the Seychelles microcontinent at ~63.4 Ma (Collier et al. 2008; Torsvik et al. 2013; review in Misra et al. 2014). By this time, during the Maastrichtian to Paleocene, the Barmer basin had matured into a long, narrow continental rift basin possibly guided by preexisting, nearly north/NNW-trending fractures of the Proterozoic MIS at ≥45° to the nearly NE-trending extension direction. This points to rifting of a more oblique nature (Bonini et al. 1997; Chattopadhyay and Chakra 2013) in the Barmer basin than the orthogonal rifting suggested by Bladon et al. (2015). Extension related to this oblique rifting between the West Indian margin and the Seychelles microcontinent (Misra et al. 2014) initiated much earlier in the Barmer basin and propagated south/SE into the Cambay basin and farther south. The Barmer basin deepens toward the south to SE, and the eastern margin accommodates sediments thicker than those at the western margin (fig. 1*e* in Bladon et al. 2014; fig. 6 in Dolson et al. 2015), making rifting more asymmetric (Huismans and Beaumont 2002). Also, the western margin is more uplifted than the eastern margin (fig. 1*C*). Oblique extension associated with preexisting structures can also rift asymmetrically (Withjack and Jamison 1986; Bonini et al. 1997, 2016; van Wijk 2005).

Conclusions

The Barmer basin is a narrow, failed continental, nonvolcanic rift region. Passive rifting was coeval with upwelling of magma under high crustal straining. Key conclusions are as follows.

1. Bladon et al. (2015) referred to two phases of extension: (1) Early Cretaceous NW-SE extension

and (2) Late Cretaceous to Paleocene NE-SW extension, which we support from field structural evidence. Bladon et al. (2015) also identified relay ramps from seismic sections in the northern and eastern parts of the Barmer basin. We present for the first time from the field such transfer zones in megascale from remote-sensing images (figs. 3*d*, 21) and document fractures that connect those ramps (figs. 20*b*, 21, A12).

2. The second-phase extension is manifested at both the western and eastern rift shoulder margins of the Barmer basin. Strain localized in the western shoulder in outboard areas farther from the rift margin. Northeast-trending faults of probably the first phase cut by NW-trending faults of the second phase observed near the Gehnoo and Dhorimana outcrops decode their relative timing.

3. Slip sense along fault planes is identified from the morphologies of slickensides and the angular relations between the Y and the P brittle planes. The NW/NNW-trending faults are dominantly dip-slip. Paleostress analysis (Zalohar and Vrabec 2007) could further interpret the relative timing among the NE- and nearly east-trending faults (results of first-phase extension) and the WNW- and NNW-trending faults (produced by second-phase extension) first documented in this study.

4. The preexisting Late Proterozoic rift fractures, trending nearly north to NNW, in the Malani Igneous Suite have plausibly favored the NE-SW main Barmer rift extension (fig. 1*A*, 1*Bi*, 1*Biii*).

5. The SSW- to WSW-trending faults in the Sarnoo hill area at the eastern margin possibly indicate a clockwise rotation of the first phase of extension during the Early Cretaceous. Paleostress analysis can confirm this. Synsedimentary growth observed along some of the SW- to WSW-trending faults, having small slip, indicate low strain. Only where distinct markers slipped did we estimate throw magnitude (Sarnoo hill area: fig. 14; NE of Sarnoo hill area: fig. 19).

6. Basalt intrusions along the Y and P brittle shear planes trending SW in the eastern Sarnoo hill area are clearly from pre-Deccan/precursor-of-Deccan volcanism at ~68 Ma.

7. Displacement of the pre-Deccan/precursor-of-Deccan basaltic sill and the overlying Early Cretaceous lower Ghaggar-Hakra sandstone by the NW-trending faults indicates that the main Barmer rift extension occurred probably during the late Maastrichtian to Paleocene period, after the pre-Deccan volcanism, during oblique rifting of the Seychelles microcontinent from India.

8. Relay structures play an important role in fault propagation, guided by the preexisting rift fractures (fig. 1*Bii*, 1*Biii*). This is also observed in the Barmer rift basin.

9. Bladon et al. (2015) documented two noncoaxial phases of extension from the Barmer basin solely on the basis of seismic fault interpretation. They suggested that the second phase of NE extension was an orthogonal rifting. However, we conclude that the main rifting during the Late Cretaceous–Paleocene was oblique in nature.

10. Bladon et al. (2015) neither documented deformation in the Malani rocks nor linked it with the subsequent Barmer basin genesis. In contrast, we decipher that the Proterozoic rift fractures in the Malani rocks controlled evolution of the Barmer basin, a kind of structural inheritance.

11. Synsedimentary growth within Early Cretaceous sandstones increases the chances of finding good Mesozoic structural reservoirs within the Barmer basin. The presence of a fault gouge (fig. 16 in the Sarnoo hill area (and elsewhere) also indicates the likelihood of finding fault-bound traps, controlled by dip-sealing faults in subsurface Mesozoic stratigraphy.

ACKNOWLEDGMENTS

S. Dasgupta thanks his wife, Troyee Dasgupta, for assisting in his first fieldwork in Barmer. S. Mukherjee thanks his wife, Payel Mukherjee, for taking care of household activities and providing free time to do fieldwork with S. Dasgupta and to partially write this article. Both the authors conducted fieldwork with their own money. A research sabbatical provided by the Indian Institute of Technology Bombay to S. Mukherjee for the year 2017 has been quite beneficial in finishing this article. S. Dasgupta is thankful to his colleagues at Reliance Industries for some valuable discussions that were beneficial while writing the manuscript. V. Gahalaut clarified the fault-plane solution, and that helped us to understand the tectonics and structures of the Barmer basin. We thank the anonymous reviewer for a constructive review and D. Rowley and B. J. Sivertsen for punctual editorial support.

REFERENCES CITED

Abdelaziz, S.; Leem, J.; Praptono, A. S.; Shankar, P.; Mund, B.; Gupta, A. K.; Goyal, R.; and Sidharth, P. 2016. An integrated workflow to the success of complex tight-gas reservoirs development north of India: case study. International Association of Drilling Contractors/Society of Petroleum Engineers Asia Pacific Drilling Technology

Conference, 11th (Singapore, 2016). Accessed December 12, 2016. https://www.onepetro.org/conference-paper/SPE-180586-MS.

Anderson, E. M. 1905. The dynamics of faulting. Trans. Edinb. Geol. Soc. 8:387–402.

Arora, K.; Suman, K.; Dixit, M. M.; and Sarkar, D. 2011. Jaisalmer basin of western Rajasthan: a gravity perspective. Geo India: South Asian Geoscience Conference and Exhibition, 2nd (Greater Noida, New Delhi, India, 2011). http://www.apgindia.org/pdf/475.pdf.

Axen, G. J., and Bartley, J. M. 1997. Field tests of rolling hinges: existence, mechanical types, and implications for extensional tectonics. J. Geophys. Res. Solid Earth 102:20,515–20,537.

Babar, M. D.; Kaplay, R. D.; Mukherjee, S.; and Kulkarni, P. S. 2017. Evidence of the deformation of dykes from the Central Deccan Volcanic Province, Aurangabad, Maharashtra, India. *In* Mukherjee, S.; Misra, A. A.; Calvès, G.; and Nemčok, M., eds. Tectonics of the Deccan Large Igneous Province. Geol. Soc. Lond. Spec. Publ. 445:337–353.

Bajpai, V. N. 2004. Hydrogeological evolution of the Luni River basin, Rajasthan, western India: a review. Proc. Indian Acad. Sci. Earth Planet. Sci. 113:427–451.

Bakliwal, P. C., and Wadhawan, S. K. 2003. Geological evolution of Thar Desert in India—issues and prospects. Proc. Indian Natl. Sci. Acad. 69A:151–165.

Baksi, S. K., and Naskar, P. 1981. Fossil plants from the Sarnu Hill Formation, Barmer Basin, Rajasthan. Palaeobotanist 27:107–111.

Bally, A. W.; Bernoulli, D.; Davis, G. A.; and Montadert, L. 1981. Listric normal faults. *In* Oceanologica acta: Geology of Continental Margins Symposium. Int. Geol. Cong., 26th (Paris, 1980), Proc. p. 87–101.

Basu, A. R.; Renne, P. R.; Dasgupta, D. K.; Teichmann, F.; and Poreda, R. J. 1993. Early and late alkali igneous pulses and a high ^{3}He plume origin for the Deccan flood basalts. Science 261:902–906.

Baudon, C., and Cartwright, J. 2008. The kinematics of reactivation of normal faults using high resolution throw mapping. J. Struct. Geol. 30:1072–1084.

Beauchamp, W.; Barazangi, M.; Demnati, A.; and El Alji, M. 1996. Intra-continental rifting and inversion: Missour Basin and Atlas Mountains, Morocco. Am. Assoc. Pet. Geol. Bull. 80:1459–1482.

Beaumont, H.; Clarke, S. M.; Burley, S. D.; Taylor, A.; Gould, T.; and Mohapatra, P. 2015. Deciphering tectonic controls on fluvial sedimentation within the Barmer Basin, India: the lower Cretaceous Ghaggar-Hakra Formation. Search Discov. 2015:51100. http://www.searchanddiscovery.com/pdfz/documents/2015/51100beaumont/ndx_beaumont.pdf.html.

Bellahsen, N., and Daniel, J. M. 2005. Fault reactivation control on normal fault growth: an experimental study. J. Struct. Geol. 27:769–780.

Bhushan, S. K. 2000. Malani rhyolites—a review. Gondwana Res. 3:65–77.

Biswas, S. K. 1987. Regional tectonic framework, structure and evolution of the western marginal basins of India. Tectonophysics 135:307–327.

———. 1999. A review of the evolution of rift basins in India during Gondwana with special reference to western Indian basins and their hydrocarbon prospects. Proc. Indian Natl. Sci. Acad. 65:261–283.

———. 2005. A review of structure and tectonics of Kutch basin, western India, with special reference to earthquakes. Curr. Sci. 88:1592–1600.

———. 2012. Status of petroleum exploration in India. *In* Banerjee, D. M., and Singhvi, A. K., eds. Glimpses of geoscience research in India: Indian report to the IUGS: 2008–2012. Proc. Indian Natl. Sci. Acad. Spec. Issue 78:475–494.

Bladon, A. J.; Burley, S. D.; Clarke, S. M.; and Beaumont, H. 2014. Geology and regional significance of the Sarnoo Hills, eastern rift margin of Barmer Basin, NW India. Basin Res. 27:636–655.

Bladon, A. J.; Clarke, S. M.; and Burley, S. D. 2015. Complex rift geometries resulting from inheritance of pre-existing structures: insights and regional implications from the Barmer Basin rift. J. Struct. Geol. 71:136–154.

Bonini, L.; Basili, R.; Toscani, G.; Burrato, P.; Seno, S.; and Valensise, G. 2016. The effects of pre-existing discontinuities on the surface expression of normal faults: insights from wet-clay analogue modeling. Tectonophysics 684:157–175.

Bonini, M.; Souriot, T.; Boccaletti, M.; and Brun, J.-P. 1997. Successive orthogonal and oblique extension episodes in a rift zone: laboratory experiments with application to the Ethiopian rift. Tectonics 16:347–362.

Brady, R.; Wernicke, B.; and Fryxell, J. 2000. Kinematic evolution of a large-offset continental normal fault system, South Virgin Mountains, Nevada. Geol. Soc. Am. Bull. 112:1375–1397.

Brune, S., and Autin, J. 2013. The rift to break-up evolution of the Gulf of Aden: insights from 3D numerical lithospheric-scale modelling. Tectonophysics 607:65–79.

Buck, W. R. 1988. Flexural rotation of normal faults. Tectonics 7:959–973.

———. 1991. Modes of continental lithospheric extension. J. Geophys. Res. Solid Earth 96:20,161–20,178.

Caine, J. S.; Evans, J. P.; and Forster, C. B. 1996. Fault zone architecture and permeability structure. Geology 24:1025–1028.

Caine, J. S., and Forster, C. B. 1999. Fault zone architecture and fluid flow: insights from field data and numerical modeling. Am. Geophys. Union 113:101–127.

Chamberlin, R. M. 1983. Cenozoic domino-style crustal extension in the Lemitar Mountains, New Mexico: a summary. *In* Chapin, C. E., and Callender, J. F., eds. New Mexico Geological Society, 34th Field Conference, Socorro Region II. Guidebook. Socorro, N. M. Geol. Soc., p. 111–118.

Chandra, U. 1977. Earthquakes of peninsular India—a seismotectonic study. Bull. Seismol. Soc. Am. 67:1387–1413.

Chattopadhyay, A., and Chakra, M. 2013. Influence of pre-existing pervasive fabrics on fault patterns during orthogonal and oblique rifting: an experimental approach. Mar. Pet. Geol. 39:74–91.

Chetty, T. R. K., and Rao, Y. J. B. 2006. The Cauvery Shear Zone, Southern Granulite Terrain, India: a crustal-scale flower structure. Gondwana Res. 10:77–85.

Chung, W. Y., and Gao, H. 1995. Source parameters of the Anjar earthquake of July 21, 1956, India, and its seismotectonic implications for the Kutch rift basin. Tectonophysics 242:281–292.

Collier, J. S.; Sansom, V.; Ishizuka, O.; Taylor, R. N.; Minshull, T. N.; and Whitmarsh, R. B. 2008. Age of Seychelles-India break-up. Earth Planet. Sci. Lett. 272: 264–277.

Collinson, J. D., and Thompson, D. B. 1984. Sedimentary structures. London, Allen & Unwin.

Compton, P. M. 2009. The geology of the Barmer Basin, Rajasthan, India, and the origins of its major oil reservoir, the Fatehgarh Formation. Pet. Geosci. 15:117–130.

Corti, G.; Bonini, M.; Conticelli, S.; Innocenti, F.; Manetti, P.; and Sokoutis, D. 2003. Analogue modelling of continental extension: a review focused on the relations between the patterns of deformation and the presence of magma. Earth-Sci. Rev. 63:169–247.

Dasgupta, S.; Pande, P.; Ganguli, D.; Iqbal, Z.; Sanyal, K.; Venkatraman, N. V.; Dasgupta, S.; et al. 2000. Thar Desert and plains of Jaisalmer-Barmer area. *In* Narula, P. L.; Acharyya, S. K.; and Banerjee, J., eds. Seismotectonic atlas of India and its environs. Calcutta, Geol. Surv. India, p. 17.

Dasgupta, S. K. 1975. A revision of the Mesozoic-Tertiary stratigraphy of the Jaisalmer Basin, Rajasthan. Indian J. Earth Sci. 2:77–94.

Davies, R.; Cloke, I.; Cartwright, J.; Robinson, A.; and Ferrero, C. 2004. Post-breakup compression of a passive margin and its impact on hydrocarbon prospectivity: an example from the Tertiary of the Faeroe-Shetland Basin, United Kingdom. Am. Assoc. Pet. Geol. Bull. 88:1–20.

Dewey, J. F.; Holdsworth, R. E.; and Strachan, R. A. 1998. Transpression and transtension zones. *In* Holdsworth, R. E.; Strachan, R. A.; and Dewey, J. F., eds. Continental transpressional and transtensional tectonics. Geol. Soc. Lond. Spec. Publ. 135:1–14.

Doblas, M. 1998. Slickenside kinematic indicators. Tectonophysics 295:87–197.

Dolson, J.; Burley, S. D.; Sunder, V. R.; Kothari, V.; Naidu, B.; Whiteley, N. P.; Farrimond, P.; Taylor, A.; Direen, N.; and Ananthakrishnan, B. 2015. The discovery of the Barmer Basin, Rajasthan, India, and its petroleum geology. Am. Assoc. Pet. Geol. Bull. 99:433–465.

Duffy, O. B.; Nixon, C. W.; Bell, R. E.; Jackson, C. A.-L.; Gawthorpe, R. L.; Sanderson, D. J.; and Whipp, P. S. 2017. The topology of evolving rift fault networks: single-phase vs multi-phase rifts. J. Struct. Geol. 96:192–202.

Dwivedi, A. K. 2016. Petroleum exploration in India—a perspective and endeavours. Proc. Indian Natl. Sci. Acad. 82:881–903.

Elliott, T. 1978. Siliciclastic shorelines. *In* Reading, H. G., ed. Sedimentary environments and facies. Oxford, Blackwell Scientific, p. 155–188.

Farrimond, P.; Naidu, B. S.; Burley, S. D.; Dolson, J.; Whiteley, N.; and Kothari, V. 2015. Geochemical characterization of oils and their source rocks in the Barmer Basin, Rajasthan, India. Pet. Geosci. 21:301–321.

Fossen, H. 2013. The role of pre-existing structures during extension of Caledonian crust and formation of the northern North Sea rift. Geol. Soc. Am. Abstr. Program 45:522.

———. 2016. Structural geology (2nd ed.). Cambridge, Cambridge University Press.

Fossen, H., and Rotevatn, A. 2016. Fault linkage and relay structures in extensional settings—a review. Earth-Sci. Rev. 154:14–28.

Gaina, C.; van Hinsbergen, D. J. J.; and Spakman, W. 2015. Tectonic interactions between India and Arabia since the Jurassic reconstructed from marine geophysics, ophiolite geology, and seismic tomography. Tectonics 34:875–906.

Gawthorpe, R. L., and Hurst, J. M. 1993. Transfer zones in extensional basins: their structural style and influence on drainage development and stratigraphy. J. Geol. Soc. Lond. 150:1137–1152.

Ghosh, S. K. 1993. Structural geology: fundamentals and modern development. Oxford, Pergamon.

Gibbons, A. D.; Whittaker, J. M.; and Müller, R. D. 2013. The breakup of East Gondwana: assimilating constraints from Cretaceous ocean basins around India into a best-fit tectonic model. J. Geophys. Res. Solid Earth 118:808–822.

Gibbs, A. D. 1984. Structural evolution of extensional basin margins. J. Geol. Soc. Lond. 141:609–620.

Gombos, A. M., Jr.; Powell, W. G.; and Norton, I. O. 1995. The tectonic evolution of western India and its impact on hydrocarbon occurrences: an overview. Tectonophysics 96:119–129.

Healy, D.; Blenkinsop, T. G.; Timms, N. E.; Meredith, P. G.; Mitchell, T. M.; and Cooke, M. L. 2015. Polymodal faulting: time for a new angle on shear failure. J. Struct. Geol. 80:57–71.

Huismans, R. S., and Beaumont, C. 2002. Asymmetric lithospheric extension: the role of frictional plastic strain softening inferred from numerical experiments. Geology 30:211–214.

John, A.; Agarwal, A.; Gaur, M.; and Kothari, V. 2017. Challenges and opportunities of wireline formation testing in tight reservoirs: a case study from Barmer Basin, India. J. Pet. Explor. Prod. Technol. 7:33–42.

Joshi, D. D.; Dharman, R.; Saxena, A. K.; and Mulkraj. 1997. Jaisalmer earthquake of 1991; its effects and tectonic implications. J. Geol. Soc. India 49:433–436.

Kaplay, R. D.; Babar, M. D.; Mukherjee, S.; and Kumar, T. V. 2017. Morphotectonic expression of geological structures in eastern part of south east Deccan volcanic province (around Nanded, Maharashtra, India). *In* Mukherjee, S.; Misra, A. A.; Calvès, G.; and Nemčok, M., eds. Tectonics of the Deccan Large Igneous Province. Geol. Soc. Lond. Spec. Publ. 445:317–335.

Kelly, M. J.; Najman, Y.; Mishra, P.; Copley, A.; and Clarke, S. 2014. The potential record of far-field effects of the India-Asia collision: Barmer Basin, Rajasthan, India. *In* Montomoli, C.; Iaccarino, S.; Groppo, C.; Mosca, P.; Rolfo, F.; and Carosi, R., eds. Himalaya-

Karakoram-Tibet Workshop, 29th (Lucca, Italy, 2014), Proc. J. Himal. Earth Sci. Spec. Vol., p. 80–81.
Kilaru, S.; Goud, B. K.; and Rao, V. K. 2013. Crustal structure of the western Indian shield: model based on regional gravity and magnetic data. Geosci. Front. 4: 717–728.
Koptev, A.; Calais, E.; Burov, E.; Leroy, S.; and Gerya, T. 2015. Dual continental rift systems generated by plume-lithosphere interaction. Nat. Geosci. 8:388–392.
Kothari, V.; Naidu, B.; Sunder, V. R.; Dolson, J.; Burley, S. D.; Whiteley, N. P.; Mohapatra, P.; and Ananthakrishnan. B. 2015. Discovery and petroleum system of Barmer Basin, India. Search Discov. 2015:110202. http://www.searchanddiscovery.com/pdfz/documents/2015/110202kothari/ndx_kothari.pdf.html.
Laul, V. 2000. Kanoi fault and its possible relation to Jaisalmer earthquakes. J. Geol. Soc. India 55:681.
Lewis, C. J., and Baldridge, W. S. 1994. Crustal extension in the Rio Grande rift, New Mexico: half-grabens, accommodation zones, and shoulder uplifts in the Ladron Peak-Sierra Lucero area. *In* Keller, G. R., and Cather, S. M., eds. Basins of the Rio Grande rift: structure, stratigraphy, and tectonic setting. Geol. Soc. Am. Spec. Pap. 291:135–155.
Lezzar, K. E.; Tiercelin, J. J.; Le Turdu, C.; Cohen, A. S.; Reynolds, D. J.; Le Gall, B.; and Scholz, C. A. 2002. Control of normal fault interaction on the distribution of major Neogene sedimentary depocentres, Lake Tanganyika, East African rift. Am. Assoc. Pet. Geol. Bull. 86:1027–1059.
Lobo, M.; Kolay, J.; Sinha, P.; Varghese, R.; Lang, C.; Kant, R.; Doodraj, S.; et al. 2015. Managing multidimensional constraints to drill ERD wells in Rajasthan with high directional difficulty index (DDI). Oil & Gas India Conference and Exhibition. Mumbai, Society of Petroleum Engineers. Accessed December 12, 2016. doi:10.2118/178073-MS.
Luhr, J. F.; Nelson, S. A.; Allan, J. F.; and Carmichael, I. S. 1985. Active rifting in southwestern Mexico: manifestations of an incipient eastward spreading-ridge jump. Geology 13:54–57.
Martino, R. D.; Guereschi, A. B.; and Montero, A. C. 2016. Reactivation, inversion and basement faulting and thrusting in the Sierras Pampeanas of Córdoba (Argentina) during Andean flat-slab deformation. Geol. Mag. 153(5–6):962–991.
Mathur, S. C. 2003. Sedimentation in Barmer Basin, Rajasthan. J. Geol. Soc. India 61:368–369.
Mathur, S. C.; Gaur, S. D.; Loyal, R. S.; Tripathi, A.; and Sisodia, M. S. 2005. Spherules from the Late Cretaceous phosphorite of the Fatehgarh Formation, Barmer Basin, India. Gondwana Res. 8:579–584.
McClay, K., and Bonora, M. 2001. Analog models of restraining stepovers in strike-slip fault systems. Am. Assoc. Pet. Geol. Bull. 85:233–260.
McClay, K. R. 1990. Extensional fault systems in sedimentary basins: a review of analogue model studies. Mar. Pet. Geol. 7:206–233.
McKenzie, D. P. 1969. The relation between fault plane solutions for earthquakes and the directions of the principal stresses. Seismol. Soc. Am. Bull. 50:595–601.
Means, W. D. 1987. A newly recognized type of slickenside striation. J. Struct. Geol. 9:585–590.
Mishra, D. C. 2011. Gravity and magnetic methods for geological studies: principles, integrated explorations and plate tectonics. Hyderabad, BS, p. 672–675.
Misra, A. A.; Bhattacharya, G.; Mukherjee, S.; and Bose, N. 2014. Near N-S paleo-extension in the western Deccan region, India: does it link strike-slip tectonics with India-Seychelles rifting? Int. J. Earth Sci. 103:1645–1680.
Misra, A. A., and Mukherjee, S. 2015. Tectonic inheritance in continental rifts and passive margins. Cham, Switzerland, Springer.
———. 2017. Dyke–brittle shear relationships in the western Deccan strike-slip zone around Mumbai (Maharashtra, India). *In* Mukherjee, S.; Misra, A. A.; Calvès, G.; and Nemčok, M., eds. Tectonics of the Deccan Large Igneous Province. Geol. Soc. Lond. Spec. Publ. 445:269–295.
Misra, A. A.; Sinha, N.; and Mukherjee, S. 2015. Repeat ridge jumps and microcontinent separation: insights from NE Arabian Sea. Mar. Pet. Geol. 59:406–428.
Misra, P. C.; Singh, N. P.; Sharma, D. C.; Upadhyay, H.; Kakroo, A. K.; and Saini, M. L. 1993. Lithostratigraphy of west Rajasthan basins. Oil and Natural Gas Commission report. Dehradun, Keshava Deva Malaviya Institute of Petroleum Exploration.
Morley, C. K. 1995. Developments in the structural geology of rifts over the last decade and their implications on hydrocarbon exploration. *In* Lambiase, J. J., ed. Hydrocarbon habitat in rift basins. Geol. Soc. Lond. Spec. Publ. 80:1–32.
———. 1999. How successful are analogue models in addressing the influence of pre-existing fabrics on rift structure? J. Struct. Geol. 21:1267–1274.
———. 2002. Evolution of large normal faults: evidence from seismic reflection data. Am. Assoc. Pet. Geol. Bull. 86:961–978.
Morley, C. K.; Gabdi, S.; and Seusutthiya, K. 2007. Fault superimposition and linkage resulting from stress changes during rifting: examples from 3D seismic data, Phitsanulok Basin, Thailand. J. Struct. Geol. 29:646–663.
Morley, C. K.; Haranya, C.; Phoosongsee, W.; Pongwappe, S.; Kornsawan, A.; and Wonganan, N. 2004. Activation of rift oblique and rift parallel pre-existing fabrics during extension and their effect on deformation style: examples from the rifts of Thailand. J. Struct. Geol. 26:1803–1829.
Morley, C. K.; Nelson, R. A.; Patton, T. L.; and Munn, S. G. 1990. Transfer zones in the East African rift system and their relevance to hydrocarbon exploration in rifts. Am. Assoc. Pet. Geol. Bull. 74:1234–1253.
Morley, C. K., and Nixon, C. 2016. Topological characteristics of simple and complex normal fault networks. J. Struct. Geol. 84:68–84.
Mukherjee, S. 2011. Flanking microstructures from the Zanskar Shear Zone, NW Indian Himalaya. YES Bull. 1:21–29.
———. 2012. Tectonic implications and morphology of trapezoidal mica grains from the Sutlej section of the

Higher Himalayan Shear Zone, Indian Himalaya. J. Geol. 120:575–590.
———. 2013*a*. Channel flow extrusion model to constrain dynamic viscosity and Prandtl number of the Higher Himalayan Shear Zone. Int. J. Earth Sci. 102:1811–1835.
———. 2013*b*. Deformation microstructures in rocks. Berlin, Springer, 111 p.
———. 2013*c*. Higher Himalaya in the Bhagirathi section (NW Himalaya, India): its structures, backthrusts and extrusion mechanism by both channel flow and critical taper mechanisms. Int. J. Earth Sci. 102:1851–1870.
———. 2014. Review of flanking structures in meso- and micro-scales. Geol. Mag. 151:957–974.
———. 2015*a*. A review on out-of-sequence deformation in the Himalaya. *In* Mukherjee, S.; Carosi, R.; van der Beek, P.; Mukherjee, B. K.; and Robinson, D., eds. Tectonics of the Himalaya. Geol. Soc. Lond. Spec. Publ. 412:67–109.
———. 2015*b*. Atlas of structural geology. Amsterdam, Elsevier.
Mukherjee, S.; Carosi, R.; van der Beek, P. A.; Mukherjee, B. K.; and Robinson, D. M. 2015. Tectonics of the Himalaya: an introduction. *In* Mukherjee, S.; Carosi, R.; van der Beek, P.; Mukherjee, B. K.; and Robinson, D., eds. Tectonics of the Himalaya. Geol. Soc. Lond. Spec. Publ. 412:1–3.
Mukherjee, S., and Koyi, H. A. 2009. Flanking microstructures. Geol. Mag. 146:517–526.
———. 2010*a*. Higher Himalayan Shear Zone, Sutlej Section: structural geology and extrusion mechanism by various combinations of simple shear, pure shear and channel flow in shifting modes. Int. J. Earth Sci. 99:1267–1303.
———. 2010*b*. Higher Himalayan Shear Zone, Zanskar Indian Himalaya: microstructural studies and extrusion mechanism by a combination of simple shear and channel flow. Int. J. Earth Sci. 99:1083–1110.
Mukherjee, S.; Mukherjee, B.; and Thiede, R. 2013. Geosciences of the Himalaya-Karakoram-Tibet Orogen. Int. J. Earth Sci. 102:1757–1758.
Naylor, M. A.; Mandl, G.; and Sijpesteijn, C. H. K. 1986. Fault geometries in basement-induced wrench faulting under different initial stress states. J. Struct. Geol. 8:737–752.
Nemčok, M. 2016. Rift and passive margins. New York, Cambridge University Press.
Nemčok, M.; Henk, A.; Allen, R.; Sikora, P. J.; and Stuart, C. 2012. Continental break-up along strike-slip fault zones; observations from the equatorial Atlantic. *In* Mohriak, W. U.; Danforth, A.; Post, P. J.; Brown, D. E.; Tari, G. C.; Nemčok, M.; and Sinha, S. T., eds. Conjugate divergent margins. Geol. Soc. Lond. Spec. Publ. 369:537–556.
Pandey, D. K., and Bhadu, B. 2010. Inter-basinal correlation of Paleogene sediments of Jaisalmer and Barmer Basins, western India: an approach by sequence stratigraphy. Biennial International Conference and Exhibition on Petroleum Geophysics, 8th. Hyderabad, Society of Petroleum Geophysicists.
Pandey, O. P., and Agrawal, P. K. 2000. Thermal regime, hydrocarbon maturation and geodynamic events along the western margin of India since late Cretaceous. J. Geodyn. 30:439–459.
Pandit, M. K.; Shekhawat, L. S.; Ferreira, V. P.; Sial, A. N.; and Bohra, S. K. 1999. Trondhjemite and granodiorite assemblage from west of Barmer: probable basement from Malani magmatism in western India. J. Geol. Soc. India 53:89–96.
Peacock, D. C. P., and Sanderson, D. J. 1991. Displacements, segment linkage and relay ramps in normal fault zones. J. Struct. Geol. 13:721–733.
Rajendran, K.; Talwani, P.; and Gupta, H. K. 1992. State of stress in the Indian sub-continent: a review. Curr. Sci. 62:86–93.
Rao, G. V. S. P.; Singh, S. B.; and Lakshmi, K. J. P. 2003. Palaeomagnetic dating of Saankra dyke swarm in the Malani Igneous Suite, western Rajasthan, India. Curr. Sci. 85:1486–1492.
Raval, U., and Veeraswamy, K. 2000. The radial and linear modes of interaction between mantle plume and continental lithosphere: a case study from western India. J. Geol. Soc. India 56:525–536.
Reeves, C. V. 2013. The global tectonics of the Indian Ocean and its relevance to India's western margin. J. Geophys. 34:87–94.
Richard, P., and Krantz, R. W. 1991. Experiments on fault reactivation in strike-slip mode. Tectonophysics 188: 117–131.
Ricketts, J. W.; Karlstrom, K. E.; and Kelley, S. A. 2015. Embryonic core complexes in narrow continental rifts: the importance of low-angle normal faults in the Rio Grande rift of central New Mexico. Geosphere 11:425–444.
Ring, U.; Betzler, C.; and Delvaux, D. 1992. Normal vs. strike-slip faulting during rift development in East Africa: the Malawi rift. Geology 20:1015–1018.
Robertson, E. A. M.; Biggs, J.; Cashman, K. V.; Floyd, M. A.; and Vye-Brown, C. 2016. Influence of regional tectonics and pre-existing structures on the formation of elliptical calderas in the Kenyan Rift. *In* Wright, T. J.; Ayele, A.; Ferguson, D. J.; Kidane, T.; and Vye-Brown, C., eds. Magmatic rifting and active volcanism. Geol. Soc. Lond. Spec. Publ. 420:43–67.
Roche, V., and van der Baan, M. 2017. Modeling of the in situ state of stress in elastic layered rock subject to stress and strain-driven tectonic forces. Solid Earth 8:479–498. doi:10.5194/se-8-479-2017.
Roy, A. B. 2003. Geological and geophysical manifestations of the Réunion Plume–Indian lithosphere interactions—evidence from northwest India. Gondwana Res. 6:487–500.
———. 2006. Seismicity in the Peninsular Indian Shield: some geological considerations. Curr. Sci. 91:456–463.
Roy, A. B., and Jakhar, S. R. 2002. Geology of Rajasthan (northwest India): Precambrian to recent. Jodhpur, Scientific, 421 p.
Ruppel, C. 1995. Extensional processes in continental lithosphere. J. Geophys. Res. Solid Earth 100:24,187–24,215.
Sanderson, D. J., and Nixon, C. W. 2015. The use of topology in fracture network characterisation. J. Struct. Geol. 72:55–66.

Schlische, R. W. 1995. Geometry and origin of fault-related folds in extensional settings. Am. Assoc. Pet. Geol. Bull. 79:1661–1678.

Sen, A.; Pande, K.; Hegner, E.; Sharma, K. K.; Dayal, A. M.; Sheth, H. C.; and Mistry, H. 2012. Deccan volcanism in Rajasthan: ^{40}Ar-^{39}Ar geochronology and geochemistry of the Tavidar volcanic suite. J. Asian Earth Sci. 59:127–140.

Sharma, K. K. 2005. Malani magmatism: an extensional lithospheric tectonic origin. *In* Foulger, G. R.; Natland, J. H.; Presnall, D. C.; and Anderson, D. L., eds. Plates, plumes, and paradigms. Geol. Soc. Am. Spec. Pap. 388:463–476.

———. 2007. K-T magmatism and basin tectonism in western Rajasthan, India: results from extensional tectonics and not from Reunion plume activity. *In* Foulger, G. R., and Jurdy, D. M., eds. Plates, plumes, and planetary processes. Geol. Soc. Am. Spec. Pap. 430:775–784.

Shelton, J. W. 1984. Listric normal faults: an illustrated summary. Am. Assoc. Pet. Geol. Bull. 68:801–815.

Sheth, H. C. 2007. Plume-related regional prevolcanic uplift in the Deccan Traps: absence of evidence, evidence of absence. *In* Foulger, G. R., and Jurdy, D. M., eds. Plates, plumes, and planetary processes. Geol. Soc. Am. Spec. Pap. 430:785–813.

Shiju, J.; Bowyer, G.; and Micenko, M. 2008. Mangala Field high density 3D seismic. Biennial International Conference and Exhibition on Petroleum Geophysics, 7th. Hyderabad, Society of Petroleum Geophysicists. https://www.spgindia.org/2008/607.pdf.

Sibson, R. H.; Robert, F.; and Poulsen, K. H. 1988. High-angle reverse faults, fluid-pressure cycling, and mesothermal gold-quartz deposits. Geology 16:551–555.

Singh, A. K., and Tewari, P. K. 2011. Infracambrian hydrocarbon systems and emerging hydrocarbon potential in Bikaner-Nagaur and Jaisalmer basins (Miajlar subbasin), Rajasthan, India. Geo India: South Asian Geoscience Conference and Exhibition, 2nd (Greater Noida, New Delhi, India, 2011). Search Discov. 2011:10324. http://www.searchanddiscovery.com/pdfz/documents/2011/10324singh/ndx_singh.pdf.html.

Sinha-Roy, S.; Malhotra, G.; and Mohanty, M. 2013. Geology of Rajasthan. Bangalore, Geol. Soc. India, 273 p.

Sisodia, M. S. 2011. Malani rhyolite: highly eroded complex crater. Curr. Sci. 101:946–951.

Sisodia, M. S., and Singh, U. K. 2000. Depositional environment and hydrocarbon prospects of the Barmer Basin, Rajasthan, India. Nafta (Zagreb) 51:309–326.

Sisodia, M. S.; Singh, U. K.; Lashkari, G.; Shukla, P. N.; Shukla, A. D.; and Bhandari, N. 2005. Mineralogy and trace element chemistry of the siliceous earth of Barmer Basin, Rajasthan: evidence for a volcanic origin. J. Earth Syst. Sci. 114:111–124.

Storey, M.; Mahoney, J. J.; Saunders, A. D.; Duncan, R. A.; Kelley, S. P.; and Coffin, M. F. 1995. Timing of hot-spot related volcanism and the breakup of Madagascar and India. Science 267:852–855.

Swanson, M. T. 1986. Preexisting fault control for Mesozoic basin formation in eastern North America. Geology 14:419–422.

Taylor, R. 2009. Ore textures: recognition and interpretation. Dordrecht, Springer, 288 p.

Torsvik, T. H.; Amundsen, H.; Hartz, E. H.; Corfu, F.; Kusznir, N.; Gaina, C.; Doubrovine, P. V.; Steinberger, B.; Ashwal, L. D.; and Jamtveit, B. 2013. A Precambrian microcontinent in the Indian Ocean. Nat. Geosci. 6:223–227.

Torsvik, T. H.; Carter, L. M.; Ashwal, L. D.; Bhushan, S. K.; Pandit, M. K.; and Jamtveit, B. 2001. Rodinia redefined or obscured: palaeomagnetism of the Malani Igneous Suite (NW India). Precambrian Res. 108:319–333.

Valdiya, K. S. 2010. The making of India: geodynamic evolution. Delhi, MacMillan.

van Hinsbergen, D. J. J.; Lippert, P. C.; Dupont-Nivet, G.; McQuarrie, N.; Doubrovine, P. V.; Spakman, W.; and Torsvik, T. H. 2012. Greater India Basin hypothesis and a two-stage Cenozoic collision between India and Asia. Proc. Natl. Acad. Sci. USA 109:7659–7664.

van Wijk, J. W. 2005. Role of weak zone orientation in continental lithosphere extension. Geophys. Res. Lett. 32:L02303. doi:10.1029/2004GL022192.

Vijayan, A.; Sheth, H.; and Sharma, K. K. 2015. Tectonic significance of dykes in the Sarnu-Dandali alkaline complex, Rajasthan, northwestern Deccan Traps. Geosci. Front. 7:783–791.

Watts, A. B. 2001. Isostasy and the origin of geological features in the continents and oceans. *In* Isostasy and flexure of the lithosphere. New York, Cambridge University Press, p. 285–300.

Wdowinski, S., and Axen, G. J. 1992. Isostatic rebound due to tectonic denudation: a viscous flow model of a layered lithosphere. Tectonics 11:303–315.

Weissel, J. K., and Karner, G. D. 1989. Flexural uplift of rift flanks due to mechanical unloading of the lithosphere during extension. J. Geophys. Res. Solid Earth 94:13, 919–13,950.

Whitney, D. L.; Teyssier, C.; Rey, P.; and Buck, W. R. 2013. Continental and oceanic core complexes. Geol. Soc. Am. Bull. 125:273–298.

Withjack, M. O., and Jamison, W. R. 1986. Deformation produced by oblique rifting. Tectonophysics 126:99–124.

Withjack, M. O.; Olsen, P. E.; and Schlische, R. W. 1995. Tectonic evolution of the Fundy rift basin, Canada: evidence of extension and shortening during passive margin development. Tectonics 14:390–405.

Withjack, M. O.; Schlische, R. W.; and Olsen, P. E. 1998. Diachronous rifting, drifting, and inversion on the passive margin of central eastern North America: an analog for other passive margins. Am. Assoc. Pet. Geol. Bull. 82:817–835.

———. 2002. Rift-basin structure and its influence on sedimentary systems. *In* Renaut, R. W., and Ashley, G. M., eds. Sedimentation of continental rifts. SEPM Spec. Publ. 73:57–81.

Wright, T. J.; Ayele, A.; Ferguson, D.; Kidane, T.; and Vye-Brown, C. 2016. Magmatic rifting and active volcanism: introduction. *In* Wright, T. J.; Ayele, A.; Ferguson, D. J.; Kidane, T.; and Vye-Brown, C., eds.

Magmatic rifting and active volcanism. Geol. Soc. Lond. Spec. Publ. 420:1–9.
Yin, A., and Taylor, M. H. 2008. Non-Andersonian conjugate strike-slip faults: observations, theory, and tectonic implications. IOP Conf. Ser. Earth Environ. Sci. 2:012026. doi:10.1088/1755-1307/2/1/012026.
Yin, Z. M., and Ranalli, G. 1992. Critical stress difference, fault orientation and slip direction in anisotropic rocks under non-Andersonian stress systems. J. Struct. Geol. 14:237–24?.
Zalohar, J., and Vrabec, M. 2007. Paleostress analysis of heterogeneous fault-slip data; the Gauss method. J. Struct. Geol. 29:1798–1810.
Ziegler, P. A., and Cloetingh, S. 2004. Dynamic processes controlling evolution of rifted basins. Earth-Sci. Rev. 64: 1–50.